UNMDP – Facultad de Ingeniería –
Departamento de Ingeniería en Materiales

Fibras de vidrio bioactivas tipo algodón con agregado de iones: investigación de Zn y Cu, y efecto combinado

Ian Heit Rimoli

DNI 41.149.008 - Legajo 12138

ianheit1998@gmail.com

Dr. Aldo Boccaccini – Dr. Gustavo Abraham

Proyecto Final para optar al grado de Ingeniero en Materiales

Mar del Plata, Marzo, 2023

UNMDP – Facultad de Ingeniería –
Departamento de Ingeniería en Materiales

Fibras de vidrio bioactivas tipo algodón con agregado de iones: investigación de Zn y Cu, y efecto combinado

Ian Heit Rimoli

DNI 41.149.008 - Legajo 12138

ianheit1998@gmail.com

Dr. Aldo Boccaccini – Dr. Gustavo Abraham

Proyecto Final para optar al grado de Ingeniero en Materiales

Mar del Plata, Marzo, 2023

Universidad Nacional de Mar del Plata- Facultad de Ingeniería

Friedrich-Alexander Universität Erlangen-Nürnberg

COTTON-LIKE ION-DOPED BIOACTIVE GLASS FIBERS: INVESTIGATION OF ZN AND CU COMBINED EFFECT

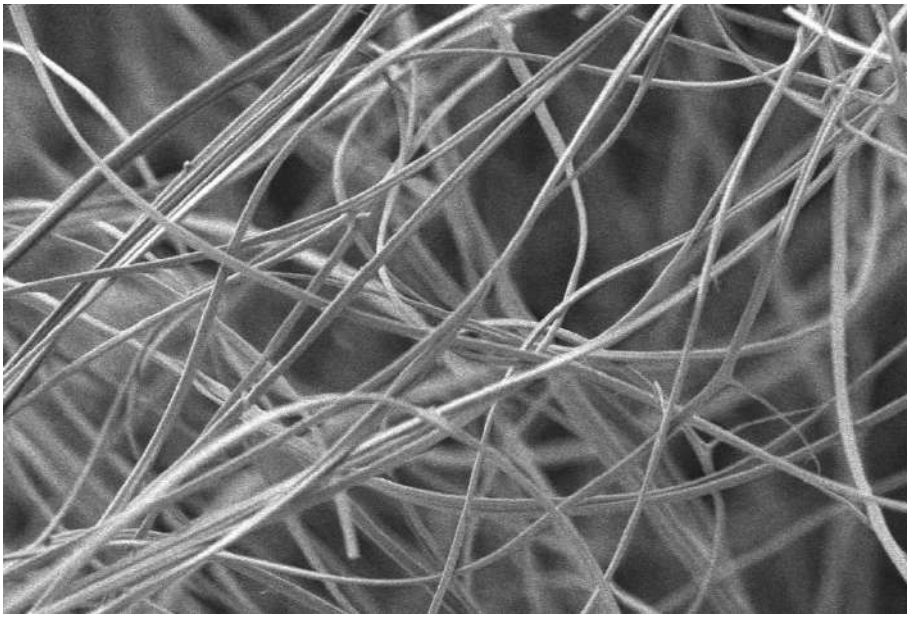

Degree's thesis

in "Materials Engineering"

Ian Heit Rimoli

Directors

Prof. Dr.-Ing. habil. Aldo R. Boccaccini

Dr. Gustavo Abraham

Dr. Liliana Liverani

Dr. Irem Ünalan

INDEX

List of figures

List of tables

List of Equations

Resumen

La ingeniería de tejidos (TE) es un campo interdisciplinario que aplica principios de ingeniería y ciencias de la vida utilizando células, biomateriales y factores físicos o moleculares, solos o en combinación, para reparar o sustituir tejidos biológicos con el fin de mejorar una respuesta clínica. Uno de los grandes retos de la ingeniería de tejidos es imitar morfológica, arquitectónica y funcionalmente la matriz extracelular (ECM, por sus siglas en inglés). En los últimos años se ha incrementado el estudio de los nanomateriales, en particular de las nanofibras, en busca de mejores soluciones a los problemas anteriormente mencionados. Los andamios de nanofibras son materiales con estructuras adecuadas para aplicaciones de regeneración cutánea o cicatrización de heridas. Se trata del uso de matrices en las que se pueden sembrar células in vitro y éstas pueden generar la ECM.

El electrohilado es una técnica versátil y sencilla que mediante la aplicación de fuerzas electrostáticas produce fibras de diámetros nanométricos o submicrónicos. Mediante esta técnica se pueden producir andamiajes nanofibrosos, con las correspondientes optimizaciones de parámetros de la solución, del proceso y de las condiciones ambientales.

En este trabajo se presenta la preparación y posterior caracterización química, morfológica y biológica de andamiajes de vidrio bioactivo en el sistema sol-gel SiO_2-CaO, un biomaterial con una elevada superficie reactiva, obtenidos mediante la técnica de electrohilado. Los parámetros de electrohilado, así como los parámetros ambientales y las correcciones en la composición resultaron los factores determinantes para la obtención de estructuras 3D "*similares al algodón*". Se hizo especial énfasis en la adición de iones de zinc y cobre al sistema de sílice y calcio, donde se estudió la influencia de estos iones en las propiedades y características de las nanofibras. Estos materiales son de especial interés en aplicaciones de cicatrización de heridas.

1. Summary

Tissue engineering (TE) is an interdisciplinary field that applies engineering and life science principles using cells, biomaterials, and appropriate physical or molecular factors, alone or in combination, to repair or replace biological tissues to improve clinical response. One of the great challenges of tissue engineering is the morphological, architectural and functional imitation of the extracellular matrix (ECM). Over the last years, the study of nanomaterials, specifically nanofibers, has increased in search of better solutions to the problems previously mentioned. Nanofibrous scaffolds are materials with structures suitable for skin regeneration or wound healing applications. It involves the use of matrices where cells can be seeded in vitro, and these can generate the ECM.

Electrospinning is a versatile and simple technique that through the application of electrostatic forces produces fibers of nanometric or submicron diameters. Nanofibrous scaffolds can be produced by this technique, with the corresponding optimizations of solution, processing and environmental parameters.

In this work, it is presented the preparation and subsequent characterization of bioactive glass scaffolds in the SiO_2-CaO sol-gel system, a biomaterial with a high reactive surface, obtained through electrospinning technique. The electrospinning parameters, as well as environmental parameters and corrections in the composition were the determining factors for obtaining 3D *"cotton-like"* structures. Special emphasis was placed on the addition of zinc and copper ions to the silica and calcium system, where the influence of these ions on the properties and characteristics of the nanofibers was studied. These materials are of particular interest in wound healing applications.

2. Introduction

2.1 Tissue engineering

One of the most common and costly problems in health care is the lost or failure of organs or tissues caused by a disease or accident, for example. Currently the most common treatments are transplants, surgical reconstructions, or the use of mechanical assist devices, among others. Within the transplants, one can differentiate those performed from one point in the body to another point in the same body (autograft) and those performed between two bodies of different patients (allograft). [1] Undoubtedly, these techniques have saved millions of lives over the years, however there are various limitations that restrict their application. Autografts are often expensive and painful, and even fatal in some cases. On the other hand, allografts are constantly in short supply and the patient is exposed to transmitted diseases or tissue rejection.

Since its appearance in the mid-1980s, tissue engineering (TE) has been developed to respond to all these problems mentioned, related to tissue replacements. The main objective is to overcome these deficiencies by creating suitable biological substitutes. Then, TE can be defined as a multidisciplinary field that combines engineering methods with knowledge of life sciences for the development of biological substitutes that replace, maintain, or improve the function of the original tissue, and in turn to fundamentally understand the relationship between the structures and functions of these substitutes. [2] Some of the potential applications of TE are in the fields of skin, blood vessel, cartilage, nerve, cardiovascular diseases, and soft tissues. [3]

TE is responsible for the construction of bioartificial tissues in vitro, as well as cell growth in vivo. It is capable of this from the isolation of cells from a certain patient. The cell culture is then expanded and seeded on a carrier in combination with growth factors. This carrier is a three-dimensional (3D) matrix, commonly known as a *"scaffold"*, which serves as a temporary framework, to accommodate the cells and their growth in all three dimensions. Finally, the implantation into the patient occurs. This can be better understood from the scheme in Figure 1, where the different strategic stages are differentiated.

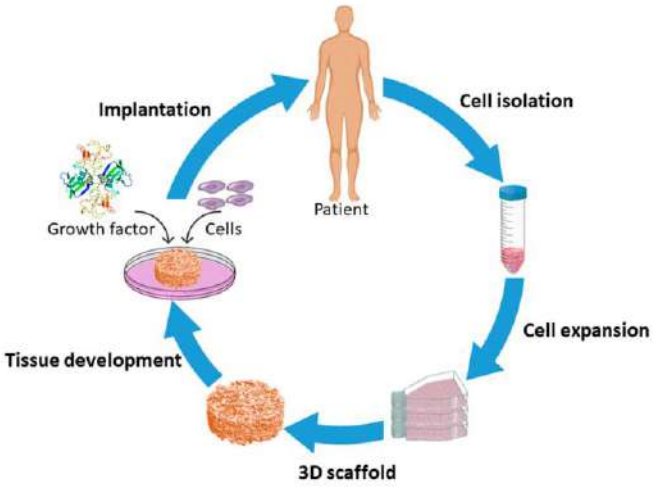

Figure 1 – Strategic stages of TE [1]

2.2 Scaffolds for tissue engineering

Most normal cells in human tissues are anchorage dependent and reside in a solid matrix, called the extracellular matrix (ECM). These ECM have different functions in the tissues, for example to give structural support to the cells so that they reside, to provide bioactive signals so that the cells respond in their microenvironment, to contribute to the mechanical properties of the tissues, to function as a reservoir for growth factors, and provide a flexible physical environment that allows remodeling from dynamic tissue processes, such as wound healing.

Ideally, the best replacement for ECM would be the same tissue in its native state, however it has been shown that it is possible to partially mimic such functionalities through the development of scaffolds. The design of a scaffold is one of the key stages in TE, and this include the multiple methods to fabricate them (extrusion, freeze-drying, rapid prototyping, molding, electrospinning), forms (nanofibers, hydrogels, mats, 3D structures, sponges, foams, membranes, nanogels) and also materials used (synthetic and natural polymers, ceramics). [4]

Certain biological, architectural, and mechanical characteristics must be taken into consideration in the development of scaffolds, among which can be highlight:

- Biocompatibility: it must integrate well to the host body, without mutagenic, carcinogenic, or cytotoxic behaviors that could cause

inflammation or major inconveniences. In other words, the immune reaction of the patient should be minimal.

- Surface properties: attachment, migration, proliferation, and differentiation of cells must be ensured.
- Biodegradability: no surgery should be necessary for implant removal, because, after certain time, native cells should be able to replace the scaffold.
- Mechanical properties: shape and mechanical stability must be provided, and also the intrinsic mechanical properties of the materials used for scaffolding should be suitable for each application.
- Architecture: porosity of the scaffold and a high surface volume ratio are important to enable cell attachment and to provide in-growth sited for cells to adhere and proliferate.

Considering these characteristics, biomaterials seem to be the best option for these demands. A biomaterial can be defined as a material used in medical applications, intended to interact with biological systems. [5] Different natural or synthetic polymers, ceramics or even composite materials can be classified as biomaterials. Natural polymers, for example, have the advantage of being normally similar to substances in the human body, but at the same time they have a degradation rate difficult to control. However, when nanometer-scale scaffolds are fabricated, new properties emerge, such as stronger mechanical capacities, lighter and more porous structures, and other significant changes related to chemical reactivity, electronic and magnetic properties, and even the appearance of new functionalities.

2.2.1 Nanofiber scaffolds

Nanostructured materials mimic the dimensions of different constituents of native tissues, such as proteins for example. One way to achieve scaffolds that comply with the previously mentioned, is to produce fibrous and porous structures. Over the last decades, development of fabrication technologies for porous scaffolds has been an intensive area of research. The concept of nanofibers and their manufacture with the appropriate production method and the proper selection of materials arise. Then, the composition, structure, and properties of nanofibers can be engineered to target specific applications,

like healthcare or biotechnology, but also energy store, environmental engineering, and defense and security.

Nanofiber mats can be designed to be morphologically and chemically similar to ECM of natural tissue, with a high surface area-volume ratio and interconnected porosity. Highly porous structures allow us to have a dynamic system where the size and shape of the pore can change. But nanofibers can also link together to form more rigid structures. [6] In particular, nanofibers can be designed to emulate as close as possible both the tensile strength and elastic modulus of human skin, while acting as a drug delivery device for wound healing therapeutics. [7]

2.2.2 Wound healing applications

The skin is the largest organ in the human body, and, as it was mentioned above, its destruction can be related with different reasons such as burns, trauma, surgery, or lacerations. In recent years, many people have suffered from chronic wounds related to diabetes, cancer, and many other causes. This is the reason why healing of wounds is currently a common concern of the global medical community. Traditional solutions for complications of this type have not been the most effective and so wound care technologies such as nanofiber scaffolds have emerged that allow skin lesions to be treated through skin tissue engineering. [8]

Wound healing can be defined as a complex physiological response of a living system to thermal, mechanical, physical, or chemical injury. Cells, scaffolds, and other biological factors combine to facilitate healing and restore the integrity of damaged tissue in the fastest and more functional and esthetic way. Some characteristics are crucial, for example, maintaining the necessary humidity in the wound bed, adaptability to the type of wound and body, temperature maintenance, gaseous exchange, prevention of microorganism colonization, biocompatibility, controlled release of therapeutic agents, non-toxicity, high reproducibility, mechanical stability, among other. [9]

In particular, a scaffold for wound healing applications must have adequate mechanical and physical properties and an excellent physiological background to allow cell adhesion, proliferation and differentiation. Additionally, a large surface area to volume ratio, an interlinked geometry, a high porosity and to be flexible enough to adapt to the shape of the wound is recommended.

Biocompatibility and biodegradability should be ensured, and ideally the degradation time of the material should be related to how long it takes for the respective wound to heal. Another important feature is to maintain a moist environment to facilitate cell adhesion, growth, and migration and to promote tissue recovery and restoration processes. Also, scaffolds can be functionalized with various agents to improve cellular responses and enhance the wound healing process.

Considering these aspects, some natural or synthetic polymers and ceramic materials emerge as attractive alternatives to be developed. Table 1 shows some examples and their most relevant properties for wound healing applications. [4]

Table 1 – Examples of biomaterials used for wound healing

Type of material	Material	Properties
Natural polymer	Collagen	Biocompatible, major protein component of ECM, high mechanical strength
	Cellulose	Biocompatible, very abundant in nature, cheaper to isolated from plant origin
Synthetic polymer	PLA	Biocompatible, biodegradable, nontoxic, structurally stable, hydrophobic
	PVA	Biocompatible, nontoxic, pH sensitive, hydrophilic, water soluble
Ceramic	Bioactive glass	Biodegradable, biocompatible, bioactive, large specific surface area in 3D structure

2.3 Electrospinning technique

There are several high-volume methods for the manufacture of nanofibers, among which are melt fibrillation, island-in-sea and gas jet, and highly precise methods like self-assembly and nanolithography. However, the combination of materials, fiber assembly, production rate, and cost are limitations to all these methods. Then, another technique called electrospinning has an important lead in terms of cost and production rate. [6]

Since the early 1990s, electrospinning is a processing technique with special interest in the field of nanoscience and nanotechnology for the manufacture of ultrafine fibers by electrically charging a suspended droplet of polymer melt or solution. The fields

of application of this technique are varied since it is possible to use a wide variety of starting materials. Compared to other manufacturing methods, electrospinning is the most widely used to make nanofiber scaffolds because of its cost-effectiveness, simple, highly versatile, and ability to be adapted for industrial scales.

The principle of electrospinning is based on the use of an electric field to drive a material solution or melt from a capillary (e.g. needle tip) to a certain collector, i.e. the formation of a solution jet. This phenomenon can be understood through a mechanism of voltage and balance of forces. When a high voltage is applied to the tip of a needle, the drop of molten material or solution is polarized, and electrical charges are induced and accumulate on the surface of the drop. Then, when the electrostatic forces overcome the surface tension of the molten material or solution, the so-called *"Taylor cone"* is formed. Figure 2 shows an example of the formation of this shape, where a cone and the following formation of multiple jets in this case are clearly observed. It is known as a cone since there is a deformation caused mainly by the electrostatic repulsions between the surface charges of the drop and the Coulomb forces caused by the strong applied electric field. If a critical value of applied electric field is exceeded, whipping motions are produced, resulting in the formation of more elongation forces which causes a greater evaporation of the solvent (or cooling of the melt) to give randomly oriented solid nanofibers in the collector. In other words, the material travels from the needle tip through the atmosphere, allowing the mentioned evaporation, and ending in the collector. Then, the mechanical properties of the material are important to prevent the breaking up of the fibers. [6] [9] [10] [11]

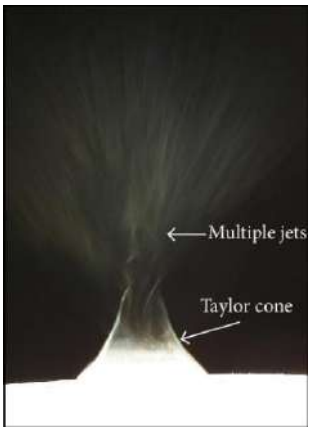

Figure 2 – Example of Taylor cone formation [12]

Figure 3 shows a general scheme of the electrospinning process, where the different parts that make up the technique are distinguished. In this representation, in the same way as in this work, a syringe pump is used which drives the syringe that contains the molten material or solution forwards through the capillary. Then it can be seen the DC supply from where the voltage is generated, and on the right the aluminum collector, where the electrospun nanofibers are being deposited. This collector is usually built from electrical conductors in order to neutralize the charge carried by the nanofibers. If the collector is shaped as in Figure 3, the nanofibers are deposited randomly, however other collector configurations (such as high-speed rotating dynamic collectors, among others) are possible with the aim of manufacturing aligned fibers.

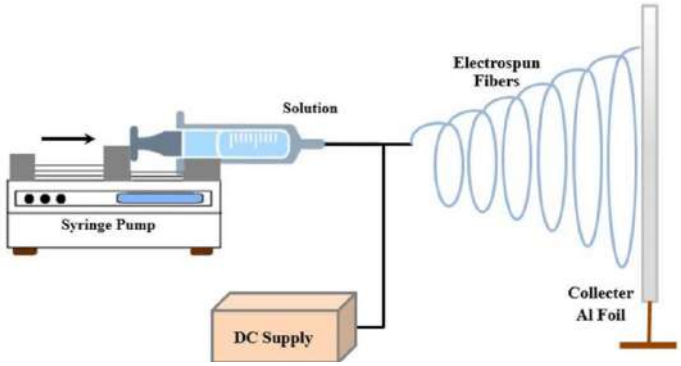

Figure 3 – Scheme of the electrospinning technique [13]

2.3.1 Fabrication parameters

There are several processing variables that are important factors for the final product obtained from this technique (morphology and properties) and for the subsequent performance of the nanofibers. The main variables are the applied voltage, the concentration and viscosity of the solution, the flow rate, the nature of the solvent, the distance between the tip and the collector, and environmental aspects such as temperature or humidity. It is important to know that the variables are dependent on each other in most cases, so they can be explained separately but must be understood as interrelated. [9]

2.3.1.1 Applied voltage

The ejection of the solution jet occurs as soon as a critical value of the applied voltage is reached. This value can be different depending on the material being used, so there is an optimal range of voltage or electric field strength depending on the type of

material-solvent in order to form nanofibers. If the voltage is higher or lower than the critical, then it results in beaded morphologies or inhibition of solution jet initiation.

Normally, as the voltage is increased above the critical, first a decrease in fiber diameter is observed, and then an increase. Initial decrease is related to the greater degree of stretching of the jet in correlation with higher repulsion of charge inside the jet and a strong external electric field. However, some studies show that such a decrease in nanofiber diameter is not necessarily always observed. It is dependent on the distance between the tip and the collector.

2.3.1.2 Distance between capillary and collector

The distance influences the size and morphology of the nanofibers. Although this effect exists, it is less relevant compared to others. In general, as the distance between the capillary and the collector increases, the fiber diameter decreases. And at short distances, it may happen that the solvent fails to evaporate completely, generating flattened structures.

2.3.1.3 Solution flow-rate

The flow rate modifies not only the diameter of nanofibers, but also their porosity and geometry. A minimum flow rate value is necessary to always have solution in the capillary and to be able to generate the jet. In case this minimum is not reached, defects can be observed since the Taylor cone shape does not remain stable. As the flow rate increases, the pore size and diameter increase as well, due to a greater volume of solution available. But when the flow rate is too high, defects are seen again since the nanofibers do not dry before reaching the collector.

2.3.1.4 Solution concentration and viscosity

The concentration of the solution modifies both the viscosity and the surface tension, with which the electrospinnability is defined with these factors. Therefore, if the viscosity of the solution is not high enough, discrete drops are formed that do not reach the collector. On the other hand, if the solution is high concentrated, the flow of the solution through the capillary is stopped. Binding agents, such as polymers, are used so

that the chain entanglement increases the viscosity of the solution and thus the fibers can be formed.

If the solution is in the appropriate concentration ranges, it has been proven that the higher the viscosity, the larger the diameter of the fibers. [9]

2.3.1.5 Conductivity

Highly conductive solutions are exposed to higher tensile forces when a voltage is applied to them, due to their higher charge capacity. This means that the higher the solution conductivities, the smaller the diameter of nanofibers. It has been experimentally verified that there is an inversely proportional relationship between the radius of the nanofibers and the electrical conductivity of the solution.

2.3.1.6 Solvent

The solvent to be chosen must be adequate so that the polymeric or ceramic material can be dissolved in it and then transformed into nanofibers by electrospinning. Also, the boiling point is of special interest due to the need for the solvent to evaporate during the manufacturing process. For example, volatile solvents facilitate the dehydration of the nanofibers during the trajectory from the capillary to the collector. But care must be taken with very volatile solvents as evaporation must not occur at the tip of the capillary, thus obstructing the flow of the material. On the other hand, solvents with very high boiling points fail to evaporate completely, thus obtaining morphological defects (such as ribbon like nanofibers) or conglutination of nanofibers at boundaries.

In addition, there is phase separation at the liquid-air interface when the jet travels towards the collector, which is a function of the volatility of the solvent and defines the porosity of the fibers. Consequently, it is also possible to use more than one solvent with two different boiling points in order to ensure that the porosity and topography are correct. Some of the most commonly used solvents are ethanol, water, chloroform, and methanol.

2.3.1.7 Temperature and humidity

Relative humidity (RH) and temperature can also modify nanofibers. According to studies, ambient humidity during electrospinning manufacturing can determine the 2D

or 3D nature of scaffolds. [14] Furthermore, a higher temperature in the room modifies the characteristics of the solution, being able to decrease the viscosity and consequently decrease the diameter of the fibers. [11]

2.4 Bioactive glasses

One of the most interesting materials for electrospinning in recent years are bioactive glasses (BG). They were invented in the 1970s and began to be used in medical applications in the 1980s. Initially, their main application was bone tissue regeneration, but they are now being applied to a wide range of tissue engineering and therapeutic purposes, such as cardiovascular tissue engineering, ocular implants, wound healing, treatment of liver cancer and ear diseases. For example, different BG systems doped with several metallic components such as Ag or Cu have been developed for wound healing and have been tested in both animals and humans, and commercial products are also available. [15]

Bioactive glasses can be defined as non-crystalline ceramics that have the ability to bond to living tissue and stimulate new tissue growth as it degrades over time. BGs can be classified according to their composition into: SiO_2-based (silicate), B_2O_3-based (borate) and P_2O_5-based (phosphate). The first ones have a wide range of developed glasses, borate glasses are characterized by higher reactivity than silicates, while the phosphate ones are resorbable materials, and their dissolution rate can be tuned according to their composition. Moreover, oxides can be added to these systems. Table 2 presents some of them, and their respective functions within the BG systems. Therefore, the potential applications are very diverse and many of them are still undiscovered. [16]

Table 2 – Oxides and their function in bioactive glasses systems

Function	Oxides
Adjust surface reactivity	CaO, Na_2O, K_2O and MgO
Improve mechanical properties	Al_2O_3
Release ions with antibacterial effects	ZnO, CuO and Ag_2O

The sol-gel process has been used to obtain BG foam or porous scaffolds, or nanoparticles; and more recently nanofibers have been electrospun for biomedical engineering applications from sol-gel solutions. [17] In other words, 3D fiber structures

can be obtained by combining the sol-gel process with electrospinning, using polymers as binding agents, and subsequent calcination.

Generally, the sol-gel process includes three stages: hydrolysis, condensation and gelation. To begin with, a chemical precursor capable of hydrolysis must be used, for example alkoxides such as tetraoxide silicon oxide (TEOS). This alkoxide is ideal as it reacts easily with water (H_2O), with the contribution of a catalyst (e.g. an acid). Then, intermediate compounds are obtained, and condensation makes it possible to create large molecules of the desired compound through polarization processes. Then, eventually, if this process continues, ramifications begin to form to the point of obtaining a gelled condition. Control over the sol-gel process is essential to obtain the desired nanofibers, since, for example, an over-gelation could cause an increase in viscosity and spinning could be affected.

3. Objectives

The main objectives of this work are:

- To explore the combined use of electrospinning and sol-gel method to produce bioactive silica-calcium glasses nanofibers.
- To analyze the electrospinning processing parameters and their interdependency.
- To design and to prepare bioactive glass nanofibers with the addition of Zn and Cu ions.
- To characterize the morphology, microstructure and chemical properties of the produced nanofibers.
- To study the bioactivity of nanofibers, with and without added ions.
- To evaluate the antibacterial activity of the nanofibers in relation with Zn and Cu presence.

4. Materials and methods

Bioactive glasses of the SiO_2 system with CaO doped with Zn and Cu ions were prepared. Sol-gel and electrospinning processes were used to fabricate the cotton-like 3D nanofibers, following the investigation started by Norris E. and Ramos C. [15], adding the mentioned ions to study changes in the antibacterial, morphological, surface and chemical characteristics.

4.1 Solution materials

TEOS (silicon tetroxide, $Si(OC_2H_5)_4$) was used as a precursor alkoxide for the sol-gel process. Nitric acid (HNO_3) was utilized as catalyst to obtain silicon dioxide (SiO_2) from TEOS (tetraethyl orthosilicate, $SiC_8H_{20}O_4$). Additionally, ethanol (C_2H_5OH) was added to the solution as a solvent required for electrospinning. Both distilled water and ethanol were available in the laboratories, while TEOS was purchased from Sigma-Aldrich and nitric acid from VWR.

To form the silica-calcium system, calcium nitrate tetrahydrate ($Ca(NO_3)_2.4H_2O$) was incorporated into the solution. In order to obtain a desired viscosity for the subsequent ES process, polyvinyl butyral (PVB) was added as a binding agent. [15] All these materials were purchased from Sigma-Aldrich (Germany).

Finally, zinc nitrate hexahydrate ($Zn(NO_3)_2.6H_2O$) and copper nitrate hemi-penta hydrate ($Cu(NO_3)_2.2,5H_2O$) were added to incorporate the ions. As with the other supplies, they were also purchased from Sigma-Aldrich (Germany).

4.1.1 Nanofibers composition

Different compositions are studied depending on the varying amounts of zinc, copper, and calcium. These are detailed in Table 3, which also shows the amount of each material used in every of the fabricated nanofibers. Formulations were named considering the composition, i.e.: “80Si20Ca” should be understood as a system of 80% silica and 20% calcium (in moles).

To calculate the amounts in grams necessary for the preparation of the solution, the molecular weight values (g/mole) provided by the supplier of each constituent were

taken. These are: 297.49 g/mole for zinc nitrate, 232.59 g/mole for copper nitrate and 236.15 g/mole for calcium nitrate.

Table 3 – Compositions for solution preparation

Composition	**$Ca(NO_3)_2.4H_2O$ (g)**	**$Zn(NO_3)_2.6H_2O$ (g)**	**$Cu(NO_3)_2.2,5H_2O$ (g)**
80Si20Ca	2.18	0	0
80Si18Ca2Zn	1.95	0.27	0
80Si18Ca2Cu	1.95	0	0.21
80Si16Ca2Zn2Cu	1.74	0.27	0.21
80Si15Ca5Zn	0.82	0.34	0
80Si15Ca5Cu	0.82	0	0.27
80Si10Ca5Zn5Cu	0.54	0.34	0.27
80Si10Zn10Cu	0	0.68	0.54

4.2 Solution preparation

The solution preparation process is described below, with the quantities required to produce 80Si20Ca (i.e. reference case). Moreover, the pertinent clarifications are made for compositions that do include Zn or Cu.

The following components were incorporated using pipettes into a small container with lid. The amount of each is related to the research of Norris E. and Ramos C. [15] Also, they were added in the following order:

1. H_2O → 0.15 ml

2. Ethanol → 2.1 ml

3. HNO_3 → 0.95 ml

4. TEOS → 4.1 ml

After 1 hour of magnetic stirrer (selected method for mixing the components), calcium was added, using an analytical balance to calculate weights:

$Ca(NO_3)_2.4H_2O$ → 1.05 g

If ions need to be added, the correct amount of each component must be calculated (see Table 3 above), and then added one by one, waiting until the previous one is

dissolved. Although there is no specific restriction to add the nitrates in a certain order, it was preferred to have experimental consistency and always add calcium first, then zinc and finally copper.

The solution is then left for 24 hours under the magnetic stirring. Once this procedure is completed, the solution is left to stand for 24 hours. Both stages were carried out with the stirrer and the resting trays inside the laboratory fume hood. Then, PVB is incorporated in the following amount:

PVB 5 w/v% → usually 0.15 g PVB with 3 ml of solution.

Then, the polymer should be dissolved, which can take between 1 to 2 hours, depending on the speed of the magnetic stirrer (the faster the stirrer, the higher the dissolution rate) and the precision when introducing the PVB into the solution. It was found that when the PVB touched the walls of the container when it was incorporated, the dissolution time increased due to the difficulty of the stirrer to mix the polymer in the walls with the liquid phase.

Once the PVB was dissolved, the solution was ready to be used for electrospinning. It worthy to note that this solution should be used immediately, otherwise the sol-gel process will continue, causing the sample to gel and consequently it will not be possible to electrospun anymore.

4.3 Electrospun nanofiber scaffolds

Once the solution was ready, it was placed in a 3 ml Henke-Ject syringe, with its respective 21G needle (0.8 mm diameter at the tip). The syringe is then placed on the pump and stabilized with tape. Flow rate was set at 0.5 ml/h. All electrospinning parameters were related to Norris et al. [15] research, but are precisely defined by Liverani et al. [18]

Moreover, the collector was covered with aluminum foil and placed in front of the needle, with a distance between the needle tip and the collector of 12 cm. In addition, a carton material is used to avoid the accumulation of nanofibers on the metal parts of the pump that could be interfering.

Finally, the power source was attached to the tip of the needle, taking care not to destabilize the syringe previously placed. Figure 4 shows the electrospinning equipment

used during the experiments; it can also be seen that it is located in a chamber with gas extraction that remove possible gases emitted during the fabrication of the nanofibers. The control panel together with the voltage generator are also showed in Figure 4.

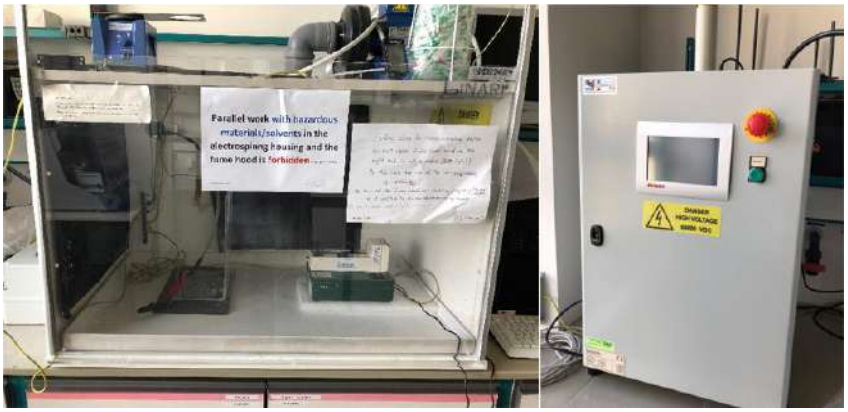

Figure 4 – Electrospinning equipment

After the set-up was ready, following the corresponding safety precautions, the voltage was activated at 15 kV and the nanofibers begin to be produced. Due to practicality issues for the collection of the fibers, they were produced for approximately 20 minutes and then the equipment was stopped. Sample collection and identification was performed, and then the voltage was turned on again. The set-up is intervened as little as possible, simply collecting the fibers, without modifying any processing parameters. The same procedure was performed repeatedly until the desired amount is produced or until less than 1 ml of solution is left in the syringe.

Figure 5 shows an example of nanofiber production, where an arc formed by the fibers, due to their own weight, can be observed.

Figure 5 – Nanofibers production using ES

An example of 80Si18Ca2Zn nanofibers production can be seen in Table 4. All fabrications details can be found in the appendix (see Section 10).

Table 4 – Fabrication of 80Si18Ca2Zn nanofibers

80Si18Ca2Zn – 07/10/2021					
ES Parameters: 15 kV – 0.5 ml/h – 12 cm					
Start time (min)	**T_o (°C)**	**RH_o (%)**	**End time (min)**	**T_f (°C)**	**RH_f (%)**
16:05	22.6	32	16:25	22.6	33
16:28	22.6	33	16:48	22.6	33
16:50	22.6	33	17:10	22.4	34
17:12	22.4	34	17:32	22.4	34
17:34	22.4	34	17:54	22.4	34

4.4 Nanofibers calcination

In order to eliminate the PVB from the nanofibers, since the polymer has already fulfilled its function as a binding agent, the fibers are exposed to a calcination heat treatment (HT) in a muffle furnace. (Nabertherm model P330, Figure 6).

Figure 6 – Nabertherm P330 used for calcination

They were placed in suitable ceramic containers, with lids to avoid contamination, and heated at 600°C at a rate of 1°C.min^{-1} with a dwell at 600°C for 3 h before being cooled naturally. [15]

4.5 Characterization

Morphological, chemical and microstructural characterization of BG nanofibers before and after calcination. FTIR, XRD, SEM and EDX studies were performed.

4.5.1 Fourier transform infrared spectroscopy (FTIR)

Infrared spectroscopy was realized using a FTIR spectrophotometer IRAffinity-1S, Shimadzu (Figure 7). Considering that the peaks in an IR spectroscopy represent the excitation of the vibrational modes of the sample molecules, the FTIR technique allows to associate these peaks to chemical bonds and functional groups present in the bioactive glasses. [19]

In this analysis, a total of 40 scans per sample were performed in absorbance mode, with a resolution of 4 cm^{-1}, Happ-Genzel type apodization (to reduce ripples) and a wavenumber range between 400 cm^{-1} and 4000 cm^{-1}.

After performing a run without a sample, to have a background spectrum, the samples were taken with tweezers and deposited directly on the device. No other previous preparation was necessary. Characterization of all compositions before and after HT was performed.

Figure 7 – FTIR IRAffinity-1S Shimadzu

4.5.2 X-Ray diffraction analysis (XRD)

X-ray diffraction (XRD) tests are based on the ability of crystals of a certain material to diffract X-rays in a characteristic way, which allows studying the structure of the crystalline phases. Furthermore, other aspects can be investigated regarding the position of the peaks, such as chemical composition, lattice parameters, among others. [20]

In this work, Rigaku Miniflex 600 equipment was used (Figure 8), with 0.020°/step, a step rate of 4°/min and a range of 6°-70°. The nanofibers had to be taped and flattened on the sample holder of the equipment, as it is important that the surface remains smooth during the test to obtain valid results. The three-dimensionality of the scaffolds was disadvantageous in this case. Fibers were analyzed before and after HT.

Figure 8 – XRD Rigaku Miniflex 600

4.5.3 Scanning electron microscope (SEM)

Using a scanning electron microscope (SEM), the morphology and microstructural characteristics can be analyzed. High quality and micro-scale images are obtained, where the diameter of the fibers can be analyzed on ImageJ software (50 fibers per composition). [21]

An Auriga-Base 0750 equipment (Zeiss, Germany) was used to examine samples, with a voltage acceleration of 1 kV, and a variable working distance depending on the sample (between 2.5 mm and 6 mm). The nanofibers were analyzed before and after calcination heat treatment.

4.5.4 Energy dispersive X-Ray analysis (EDX)

Using the same equipment as for SEM (Auriga-Base 0750), energy dispersive analysis was performed, with the main objective of determining the chemical elements present in the electrospun bioactive glass samples and their respective relative concentration. Also, this technique is used to analyze the spatial distribution of elements by making color maps of a certain region in the sample selected.

A voltage acceleration of 20 kV was applied and the working distance was modified according to the sample to be analyzed (between 5-6 mm). In this case, EDX study was performed only after HT.

4.6 Simulated body fluid test

In order to test the capability of a material to bone-bonding, the formation of apatite on the surface is examined when the material is immersed in a simulated body fluid (SBF), that is designed to be equivalent to the human blood plasma. After several investigations, it was concluded that the formation of apatite in the materials is useful for predicting bone bioactivity *in vivo*, largely decreasing the need for animal experiments. [22]

Then, SBF should be prepared with the inorganic constituents of human blood plasma and with a pH similar to that present in the body, in order to simulate an in vivo environment. Figure 9 shows the set up for the preparation, where a pH meter and a magnetic stirrer with hot plate are necessary to adjust the parameters. During the process it must be considered that SBF is a supersaturated solution with respect to apatite, and its precipitation must be avoided, so controlling that the SBF remains colorless and transparent is fundamental. If this is not the case, the solution must be disposed of and prepared again.

The preparation consists of introducing different reagents step by step into a container of distilled water, waiting for a certain period of time until the previous one was dissolved. These reagents have the function of simulating the components of human blood plasma, incorporating ions into the solution. Temperature and pH must be carefully controlled permanently.

Figure 9 – SBF preparation set up

The reagents added were NaCl, $NaHCO_3$, KCl, $K_2HPO_4.3H_2O$, $MgCl_2.6H_2O$, $CaCl_2.2H_2O$, Na_2SO_4 (all purchased from Sigma-Aldrich and VWR Chemicals). Also, HCl and Tris were used to buffered at desirable pH. The final pH must be between 7.42-7.45, and the temperature of the solution should not exceed 36.5°C during the process. The SBF solution should be stored in a refrigerator for a maximum of 30 days.

A puncher is used to form cylindrical samples (diameter of 3 mm). The sample amount is defined according to the equation Vs=Sa/10 (where Vs is SBF volume in ml, Sa is external surface area of the sample in mm^2). [22] In this case, an average of 15 ml SBF volume was used, due to the small variation in specimen sizes.

Nanofiber samples were immersed in SBF for 1, 3 and 7 days at 37°C and 100 rpm in an orbital shaker incubator (simulating physiological temperature). In total, twelve samples of each fabricated nanofiber composition (after HT) were tested. The sample must be wash with pure water after the immersion and dried in a desiccator without heating. XRD and FTIR tests are proposed to evaluate the presence of apatite.

4.7 Antibacterial test

The antibacterial activity of the scaffolds was tested against gram-positive bacteria *S. aureus* and gram-negative bacteria *E. coli*., due to the interest in studying this characteristic as a function of the amount of Zn or Cu ions present in the nanofibers.

The scaffolds were sterilized with UV irradiation for 30 min each side. On the other hand, for 24 hours at 37°C, bacteria colonies were incubated in 10 ml of Luria/Miller

medium (LB medium; Carl Roth, Germany). Then, the optical density (OD) of the bacteria population was calibrated (600 nm, Thermo Scientific™ GENESYS 30™, Germany) to reach the value of 0.001 nm, according to bacterial turbidity measurement cultures. Afterward, a volume of 1 mL inoculum of *S. aureus* and *E. coli* was added to each sample and incubated at 37 °C for 24 hours. To measure the metabolic activity of bacteria, Alamar blue (Invitrogen, United States) was added after 24 hours and incubated according to the manufacturer's protocol.

Afterwards, absorbance measurements at 570 and 600 nm were performed (region of interest for this type of bacteria), and the reduction of Alamar blue was calculated using the following Equation 1.

$$Reduction\ of\ Alamar\ Blue\ reagent\ [\%] = \frac{(E_{oxi,600} * A_{570}) - (E_{oxi,570} * A_{600})}{(E_{red,570} * C_{600}) - (E_{red,600} * C_{570})}$$

Equation 1 – Reduction of Alamar Blue reagent

Where

- $E_{oxi,570}$ = molar extinction coefficient of oxidized Alamar Blue at 570 nm = 80586
- $E_{oxi,600}$ = molar extinction coefficient of oxidized Alamar Blue at 600 nm = 117216
- $E_{red,570}$ = molar extinction coefficient of reduced Alamar Blue at 570 nm = 155677
- $E_{red,600}$ = molar extinction coefficient of reduced Alamar Blue at 600 nm = 14652
- A_{570} = absorbance of test wells at 570 nm
- A_{600} = absorbance of test wells at 600 nm
- C_{570} = absorbance of negative control well (media, Alamar Blue Reagent, no cells) at 570 nm
- C_{600} = absorbance of negative control well (media, Alamar Blue Reagent, no cells) at 600 nm

Furthermore, the viability of incubated bacteria in contact with the samples was assessed using agar plates (LB Agar; Carl Roth, Germany). The growth of bacteria was observed after 24 hours of incubation at 37°C after plating 100 µl of supernatant onto agar plates. As a control, bacteria were cultured without scaffolds. The experiments were carried out in triplicate for all the compositions, only after HT.

4.7.1 Bonferroni test

In order to adjust the significance level of the experimental tests performed, the Bonferroni statistical method is applied. In other words, when multiple trials are performed, the probability of committing false positive errors (type I error) may increase, which can lead to poor results. The method is based on the Bonferroni inequality, which states that the probability of making at least one type I error in k independent trials cannot be greater than k times the desired significance level. [23] The significance level is the value established to determine if a result is statistically significant or not, i.e. whether a result is due to chance or not. For example, if the level is 0.05, it would mean that there is less than 5% probability that the results are due to chance.

The Bonferroni test was performed for all the results using Origin Pro 8 software. Taking into account the characteristics of the method, the results of the antibacterial test were evaluated with significance levels of 0.05, 0.01 and 0.001.

5. Results and discussion

5.1 Electrospun nanofiber scaffolds

Overall, the fabrication of all electrospun bioactive glass compositions was successful. Figure 10 shows the cotton-like appearance of the nanofibers and how they were stored for later characterization, preventing ambient factors such as temperature or humidity from affecting their structure. In this case, 80Si20Ca, 80Si18Ca2Zn and 80Si18Ca2Cu scaffolds are shown.

Figure 10 – Cotton-like electrospun nanofibers

During the fabrication of nanofibers, ES parameters were not modified, the voltage (15 kV), distance (12 cm) and flow rate (0.5 ml/h) were used in all cases. However, during the production of some compositions (80Si20Ca and 80Si15Ca5Cu) it was not possible to obtain the desired 3D structure, obtaining instead 2D films. Considering that ES parameters were kept constant, it is observed that the ambient temperature remains relatively constant while the relative humidity has some variations (see Appendix, section 10.1.1 and 10.1.6). An average RH of 28.81 ± 3.06% and an average temperature of 23.33 ± 1.15°C were measured for all the compositions. RH values ranged from 27-37% for 80Si20Ca, which can be detrimental since such low RH can affect the three-dimensionality. [15] Meanwhile for 80Si15Ca5Cu the RH was 26-28%, and 2D films only appeared occasionally. It is important to point out that, these difficulties were minimal as they only occurred for a few minutes during the fabrication of only two compositions, while with the rest there was no issues (having also worked at low relative humidity), but this parameter must be considered as an important factor for the macrostructure of nanofiber scaffolds. [15] [18]

On the other hand, another reason that could compromise the three-dimensionality of the scaffolds was the absence of Ca^{2+} in the solution, since the presence of these ions increases the charge density on the surface of the jet, and therefore by force balance within the jet they allow branching of nanofibers and formation of 3D structures. [17] Then, it was expected that the 80Si10Zn10Cu composition would be 2D or have fabrication difficulties, however this did not occur, and 3D scaffolds were obtained and could be characterized as well as the rest of the compositions.

5.1.1 Fiber morphology

SEM images were used to analyze the morphology. Starting with the reference composition, 80Si20Ca before HT, it can be seen in Figure 11 that a network of entangled nanofibers is formed. It can also be seen that some fibers do not manage to separate from each other, remaining attached. Furthermore, the nanofibers can be considered homogeneous, bead-free (i.e., no *"spherical"* agglomerations), and with an appeared smooth surface.

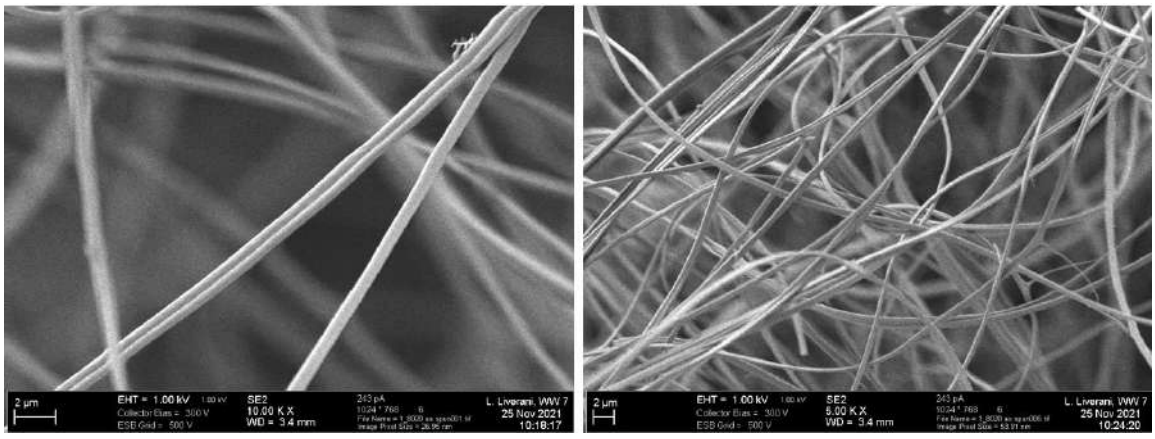

Figure 11 – SEM of 80Si20Ca before HT

Figure 12 shows the 80Si20Ca nanofibers after the calcination heat treatment, which removed the PVB component from the sample. It can be corroborated that the morphology of the fibers is not modified, nor were changes in the macrostructure detected. In this SEM image can also be seen how some fibers are held together, and some cross-cut fibers appear as well.

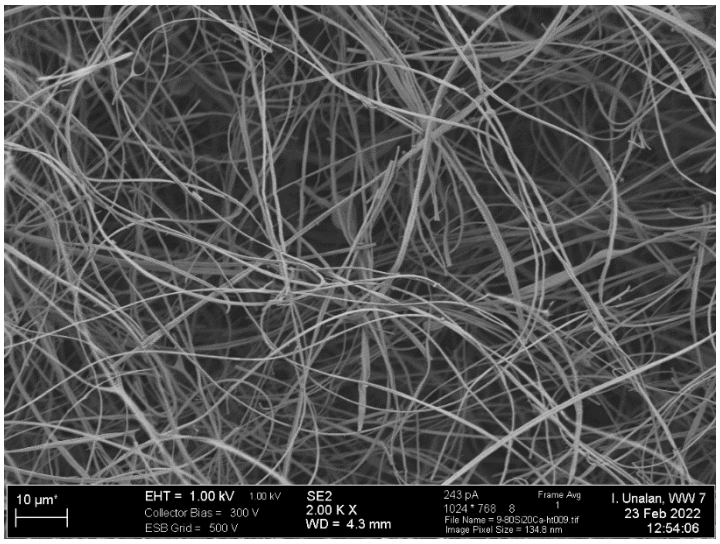

Figure 12 – SEM of 80Si20Ca after HT

In the center, right low corner, and background of Figure 13 some beads are distinguished. The beads usually appear due to the ES production process itself and/or the preparation of the solution. It was mentioned before that, for example, not using the correct applied voltage can generate beads [9]. At the same time, during the preparation of the solution, the procedures were not always identical due to occasional difficulties to dissolve the PVB (between 1-2 hours), so this longer gelation stage could be influencing the final viscosity of the solution and consequently the possible formation of beads. [15] [24]

As previously mentioned, the morphology of the electrospun fibers is controlled by the ES parameters, and also by the intrinsic properties of the solution. Within these aspects, intermolecular interactions are a determining factor, and consequently PVB as a binding agent is significantly important. Adding a long chain polymer to the sol-glass system gives the correct viscosity range to be able to produce the desired nanofibers. Not only the concentration of polymeric agent is relevant, but also the type of polymer, as this will modify the conformation of polymeric chains, elasticity, and electrical conductivity. [25]

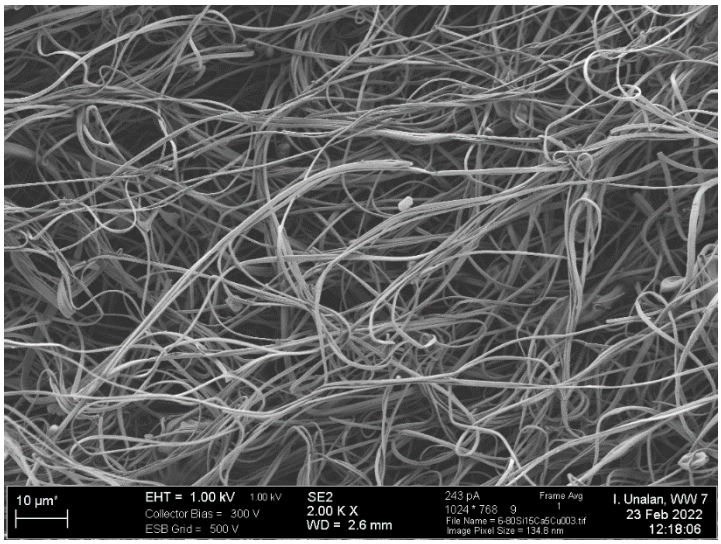

Figure 13 – SEM of 80Si15Ca5Cu before HT

In Figure 14, 80Si16Ca2Zn2Cu after HT is captured, and it can be seen that the morphology and distribution of nanofibers is not affected by adding zinc and copper ions to the solution. Highly interconnected networks of fibers of varying diameters are still visible.

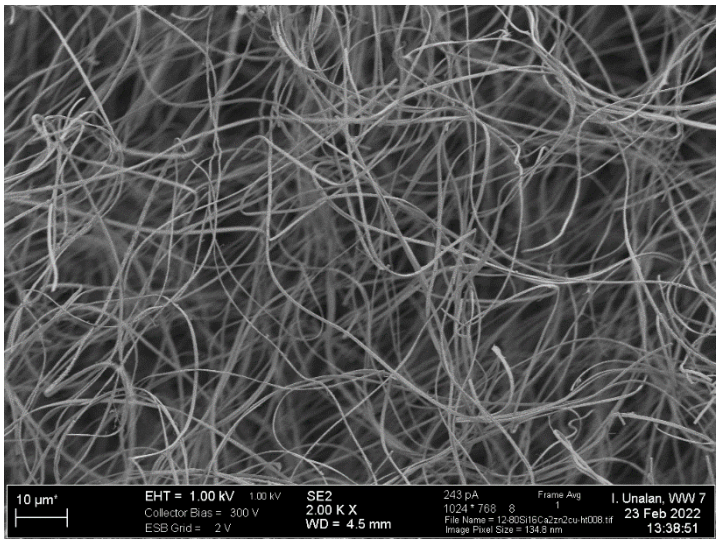

Figure 14 – SEM of 80Si16Ca2Zn2Cu after HT

In relation to the 80Si10Zn10Cu composition, without calcium (Figure 15), certain peeling of the nanofibers was observed in certain areas of the sample, giving a non-smooth fiber surface.

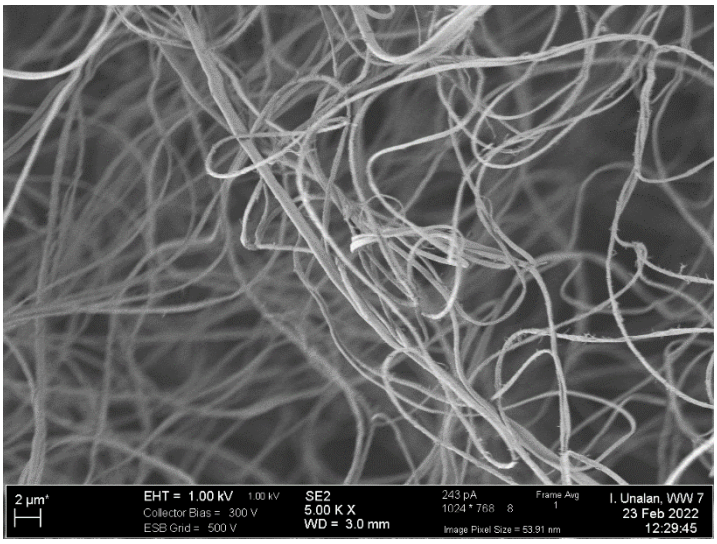

Figure 15 – SEM of 80Si10Zn10Cu before HT

This complex morphology is still visible once the sample is calcined (Figure 16), long and entangled fibers with interconnected pores can be seen.

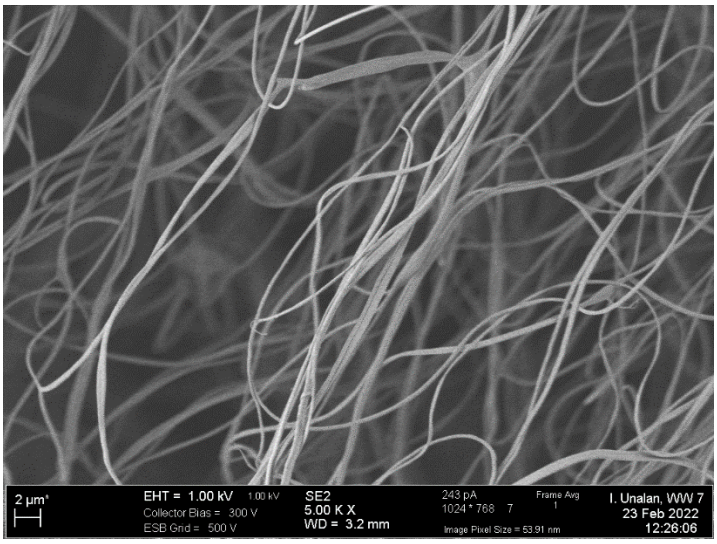

Figure 16 – SEM of 80Si10Zn10Cu after HT

To summarize, for all compositions, mostly homogeneous nanofiber scaffolds were obtained, with some occasional beads and with smooth-appearing fibers of different diameters. In addition, certain fibers were seen to stick together, even after calcination heat treatment. This is in agreement with other literature reports, where similar components were used for the production of the scaffolds. [15] [17]

5.1.2 Mean fiber diameter

Using ImageJ software [21] it was possible to analyze the average size of the nanofibers for each composition and their respective standard deviation. The results are summarized in Table 5.

Table 5 – Nanofibers mean diameter and standard deviation

	Composition	**Mean (nm)**	**Standard deviation (nm)**
Before HT	80Si20Ca	714	142
	80Si18Ca2Zn	665	156
	80Si18Ca2Cu	665	184
	80Si16Ca2Zn2Cu	600	144
	80Si15Ca5Zn	788	197
	80Si15Ca5Cu	679	262
	80Si10Ca5Zn5Cu	705	170
	80Si10Zn10Cu	592	107
After HT	80Si20Ca	621	131
	80Si18Ca2Zn	552	165
	80Si18Ca2Cu	726	256
	80Si16Ca2Zn2Cu	638	169
	80Si15Ca5Zn	702	166
	80Si15Ca5Cu	612	175
	80Si10Ca5Zn5Cu	528	133
	80Si10Zn10Cu	492	172

Figure 17 shows graphically the values obtained, grouped by equal composition. It is noted that for the same composition, there is a decrease in the average diameter of nanofibers after heat treatment. This has been reflected in previous research, where for example with 70Si30Ca compositions, diameters of 329±32 nm and 199±20 nm were reported before and after HT, respectively. [26] This behavior is related to the removal of the PVB binding polymer. In this case, the decrease is not so abrupt, and this may be related to the amount of PVB used. [17] The higher the concentration of binding polymer, the greater the decrease in diameter once the polymer is calcined.

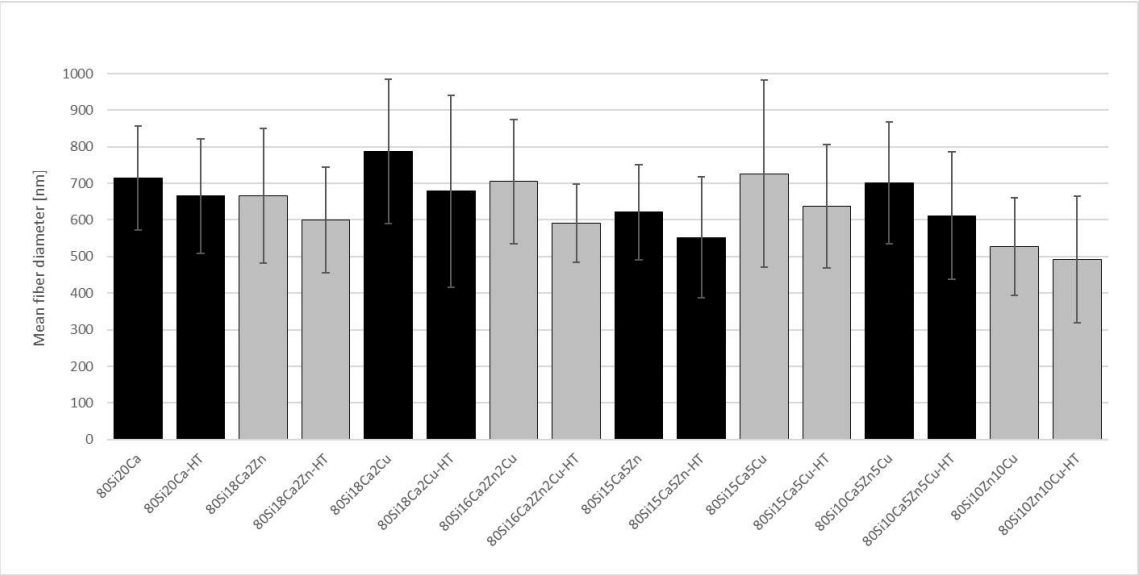

Figure 17 – Nanofibers diameters with standard deviation

Moreover, compositions with Cu (80Si18Ca2Cu or 80Si15Ca5Cu) have larger diameters than nanofibers with Zn (80Si18Ca2Zn or 80Si15Ca5Zn). In a way, this can be explained by the fact that in the Cu samples there were more fibers that remained attached, which increases the mean of the sizes analyzed with the software. This error in the measurement of the diameters is because depending on the angle of view on the fibers, it is difficult to determine whether it is a single fiber or two attached fibers. However, all the compositions are approximately in the range 500-700 nm, which is in line with other fabrications of this type of scaffolds. [18] [25]

5.2 FTIR characterization

All compositions were characterized by FTIR, before and after heat treatment. Figure 18 shows the results before HT for each of the samples. Band intensities are expressed as absorbance.

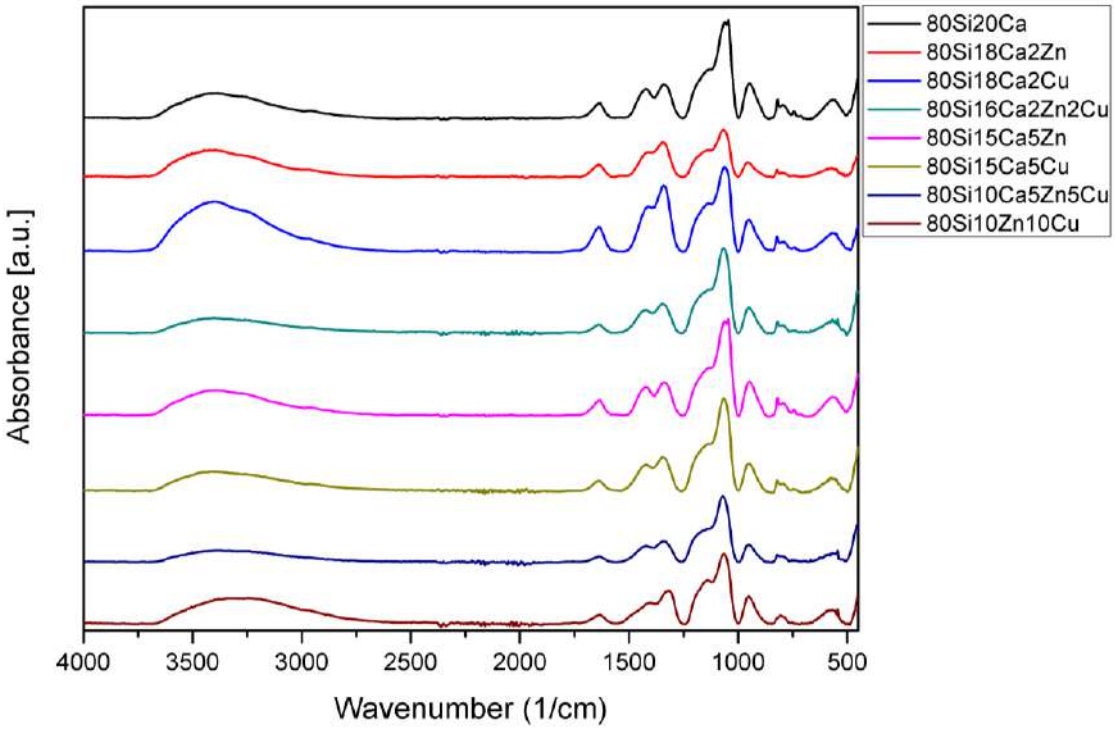

Figure 18 – FTIR spectra for each composition before HT

At first glance, it can be noted that the position of the peaks does not vary from one sample to another. This indicates that the presence of zinc and copper ions does not cause changes in the functional groups of the bioactive glasses. Furthermore, slightly different peak intensities can be seen, which may be associated with the amount of the functional group per unit volume in the sample measured.

The peaks can be identified according to literature results [15] [18], which are summarized in Table 6. Si-OH and Si-O-Si functional groups can be related to the type of silica bioactive glass manufactured. Also, C-H groups linked to the presence of PVB polymer and O-H vibrational groups due to the existence of residual water and solvents (ethanol). Figure 17 shows that these O-H peaks differ in their intensity, which infer that the amount of water and residual solvents in the samples is not necessarily the same for all samples.

Table 6 – FTIR peaks and respective functional group

Peak position (cm^{-1})	**Functional group**
803	Si-OH
953	Si-OH

1065	Si-O-Si
1140	Si-O-Si
1322	C-H
1413	C-H
1634	O-H
3324	O-H

For the samples after HT, FTIR spectra are presented in Figure 19. As in Figure 18, the peaks for each different composition are located in the same places. No peak shift was detected.

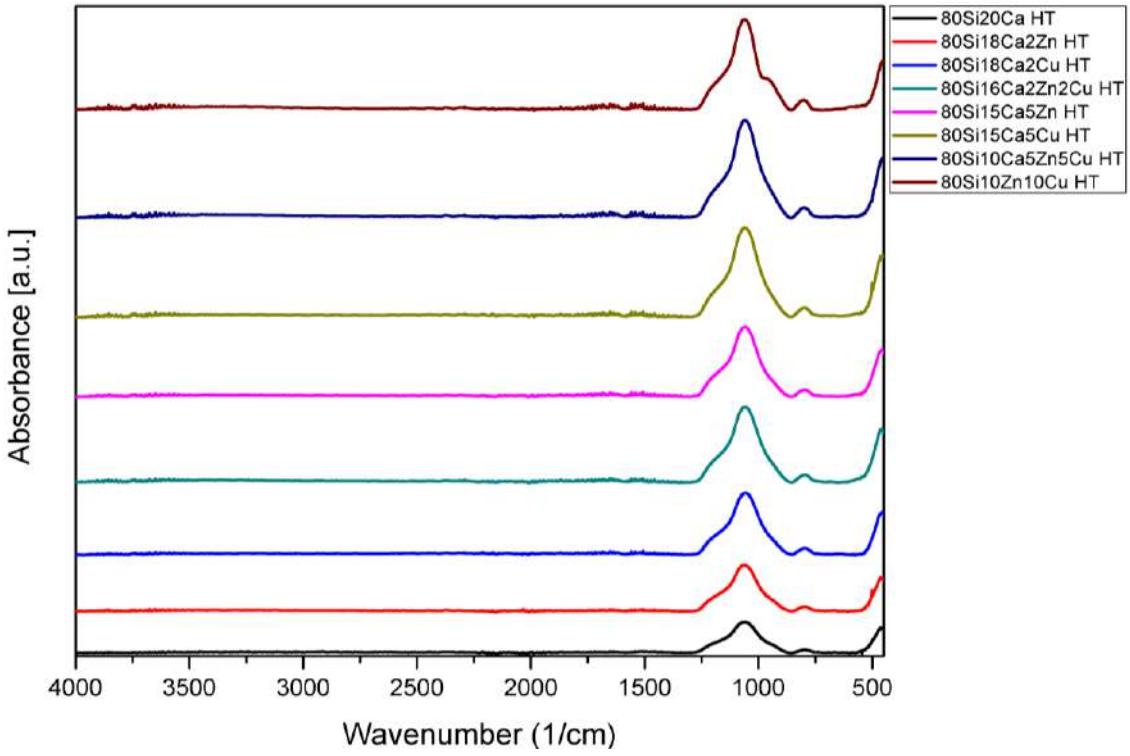

Figure 19 – FTIR spectra for each composition after HT

Once again, the different compositions did not show changes in the position of the peaks. The peaks between 950-1050 cm^{-1} and 1150 cm^{-1} linked to the Si-O-Si and Si-OH groups were still observed. On the other hand, the groups related to PVB, water and other solvents can no longer be detected, which confirms their complete disappearance during the thermal calcination treatment.

Figure 20 shows a comparison between two 80Si20Ca samples, one after HT and the other without. Here the above-mentioned absence of peaks after HT can be clearly observed.

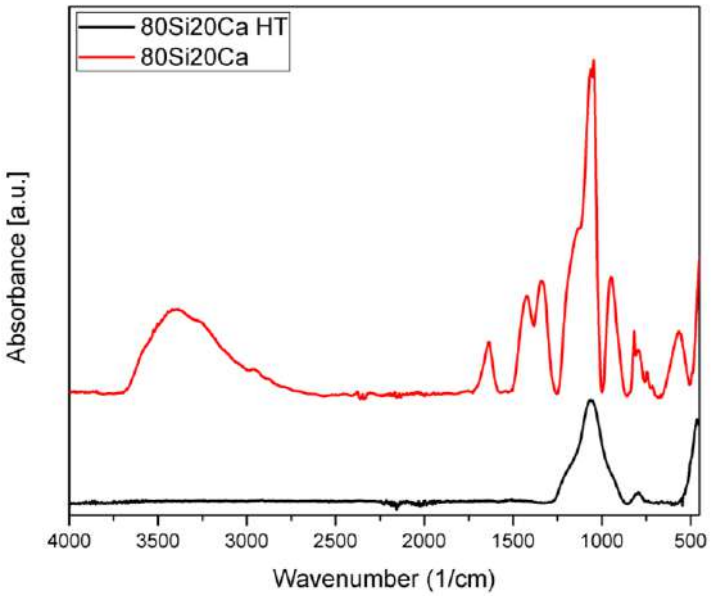

Figure 20 – Comparison of 80Si20Ca

5.3 XRD analysis

The XRD study was carried out with the aim of confirming the presence of amorphous silica, considering that we worked with bioactive glasses of the Si-Ca system. Figure 21 shows the results for the 80Si20Ca composition, before and after HT.

As can be clearly seen in Figure 21, an amorphous silica halo is not observed, as does occur in the literature. [15] [17] Three peaks associated with crystalline phases are visible. These peaks are located at 13.8°, 16.7° and 25.4°. Considering that the sample before HT is not subjected to any temperature higher than room temperature, and that HT only reaches a maximum temperature of 600°C, it is assumed that the samples were not properly prepared, which caused a contamination in the results, probably related to the preparation of the samples when they were placed inside the equipment.

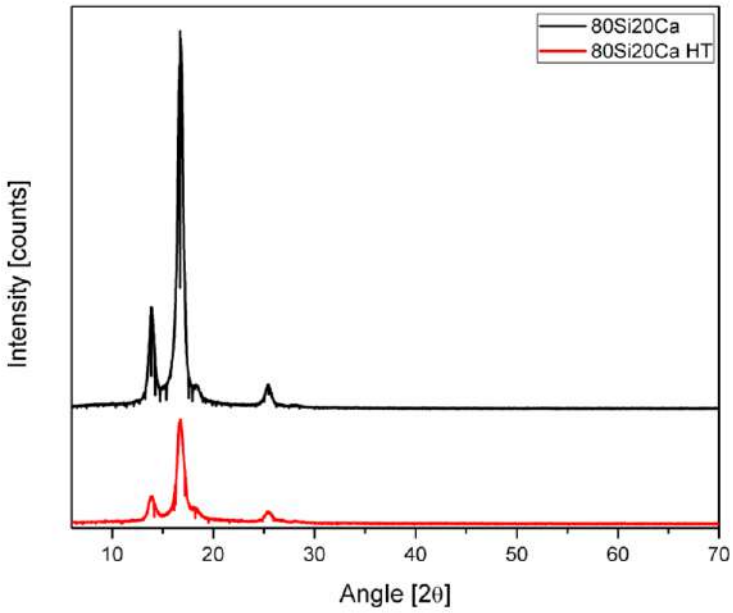

Figure 21 – XRD patterns for 80Si20Ca

Three hypotheses of possible contaminations are assumed, where the sample support material, adhesive tape and calcium nitrate are the main targets of analysis. From the database, it is found that the peaks 13.8° and 16.7° may be related to the polypropylene from which the adhesive tape used to stick the sample to the support is made. Remembering that this tape was specially used to have a flat sample inside the XRD, contamination could occur in the results due to a bad distribution of the nanofibers on the tape. In addition, the peak at 25.4° may be a crystalline phase of the silica (quartz-α), which could be explained by the fact that the sample was placed in a glass sample holder. [27] [28]

As mentioned, the peaks could also be crystalline phases of the calcium nitrate used during the preparation of the nanofibers. This hypothesis is refuted from the graph in Figure 22, where the 80Si10Zn10Cu sample has exactly the same peaks as all the other compositions. Thus, the presence of these phases, which could have appeared due to heterogeneous distribution of the component, is dismissed.

The intensity of the peaks is a factor that depends, among other things, on the crystallographic orientation, the presence of crystalline defects, the purity and size of the sample and the quality of the sample preparation, which is why differences in intensity are seen between the samples before HT and after. [20]

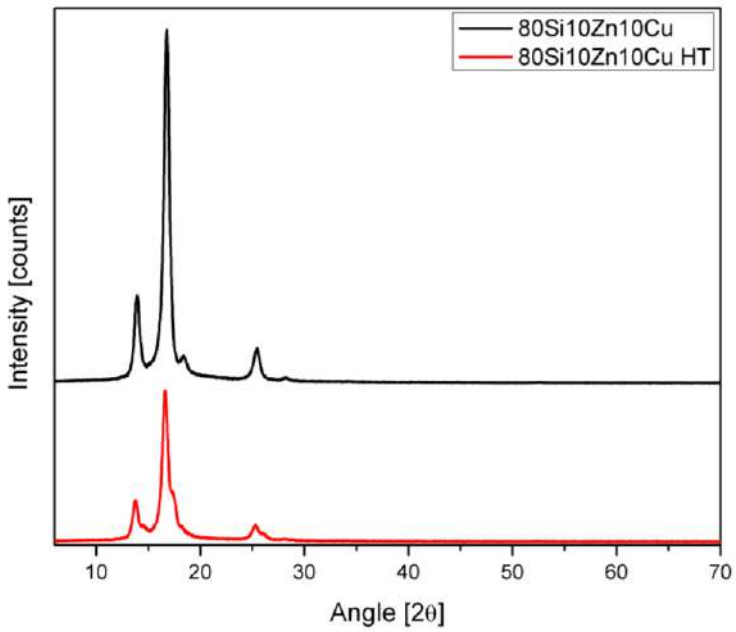

Figure 22 – XRD patterns for 80Si10Zn10Cu

5.4 EDX characterization

X-ray energy dispersive analysis was performed, and the chemical elements present in the samples, as well as their space distribution, were known. Measurements were taken at different points of each sample, since sometimes this technique confuses elements due to the fact that their energy peaks are practically overlapped. Work was done on a correct calibration and adjustment of the equipment to reduce these effects.

In general terms, all compositions showed the expected chemical elements, then some examples can be discussed in detail. Figure 23 shows the elements present in the 80Si18Ca2Cu (Figure 23 – A) and 80Si15Ca5Cu (Figure 23 – B) compositions. It is found that the sample with 5% Cu shows higher Cu energy peaks than the sample with 2%.

At the same time, Si, Ca, C and O peaks, characteristic of bioactive Si-Ca glasses, appear. The difference in intensity of these peaks between one sample and another may be due to the position from which the measurement was taken, since the distribution of the elements is not necessarily perfectly homogeneous throughout the scaffold.

Also, the intensity of the peaks verifies the proportions considered during the preparation of the nanofibers, where we have mostly Si and O (from SiO_2), Ca from calcium nitrate and finally copper in smaller quantities.

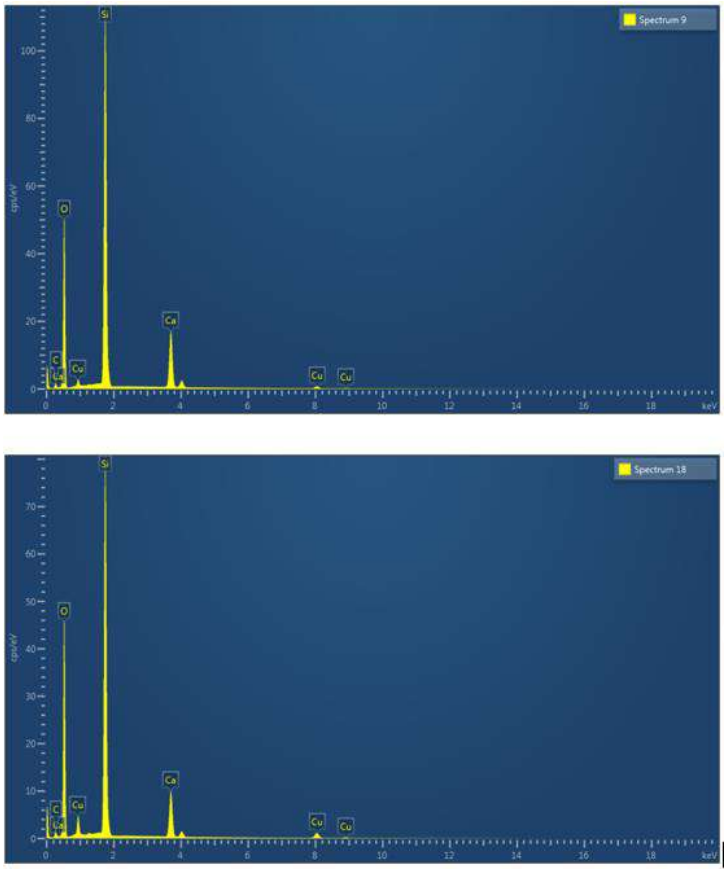

Figure 23 – EDX for 80Si18Ca2Cu (A) and 80Si15Ca5Cu (B)

On the other hand, the composition 80Si10Ca5Zn5Cu (Figure 24) shows both copper and zinc energetic peaks, confirming the presence of both ions in the nanofibers. The presence of the elements Si, Ca, O and C is also observed.

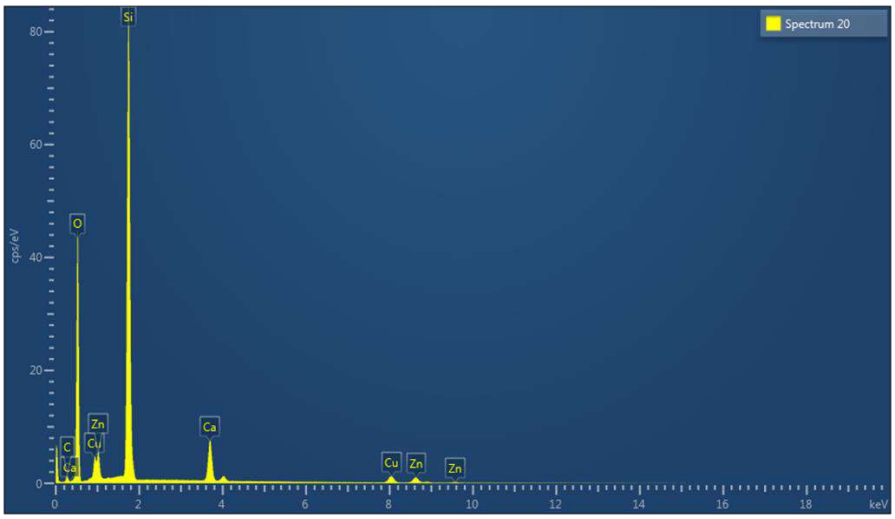

Figure 24 – EDX for 80Si10Ca5Zn5Cu

Using the equipment's software, relative concentration values are obtained (from the comparison of the peaks), i.e. a semi-quantitative study is carried out, and the following weight percent (Wt%) values are obtained (Table 7).

Table 7 – Element weight percent

Element	Wt%
O	50.88
Si	34.13
Ca	5.68
Cu	4.59
Zn	4.74

It can be verified that the composition at that point of the sample matches with the preparation made when fabricating the material (noting that 80Si10Ca5Zn5Cu is a composition defined by mole percent, and this results in Table 7 are in weight percent). Performing this analysis at different points in the sample gives results that are always approximate but never exactly the same, indicating that the distribution is not perfectly homogeneous as mentioned above.

Another interesting composition to study is 80Si10Zn10Cu (Figure 25), where in this case there are no Ca peaks, which was expected. Moreover, due to the higher amount of zinc and copper ions, their respective peaks present a higher intensity.

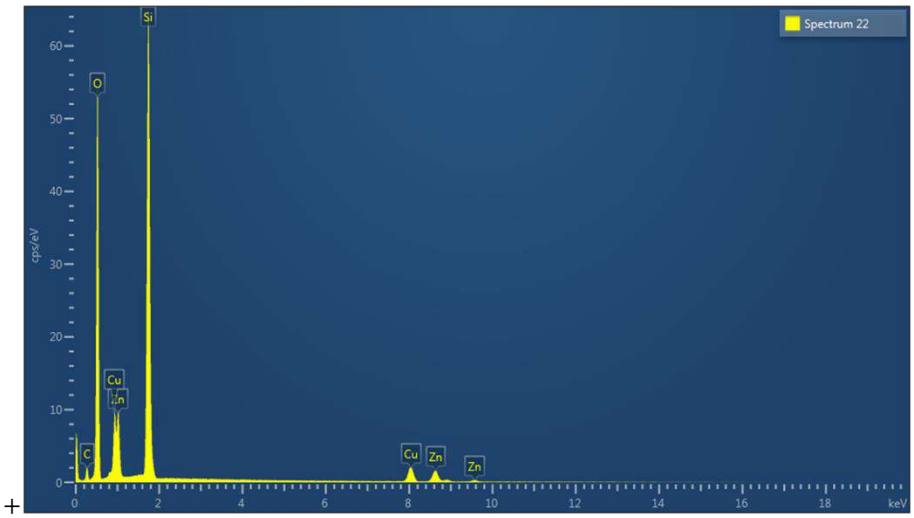

Figure 25 – EDX 80Si10Zn10Cu

The color mapping of this sample (80Si10Zn10Cu) shows the spatial distribution of the elements. Figure 26 shows these mappings, where in general terms it can be said that the distribution is relatively homogeneous but with certain areas with higher concentrations of some elements, and other regions with lower presence. The distribution was similar for the rest of the compositions, and no significant differences were detected in any of the samples.

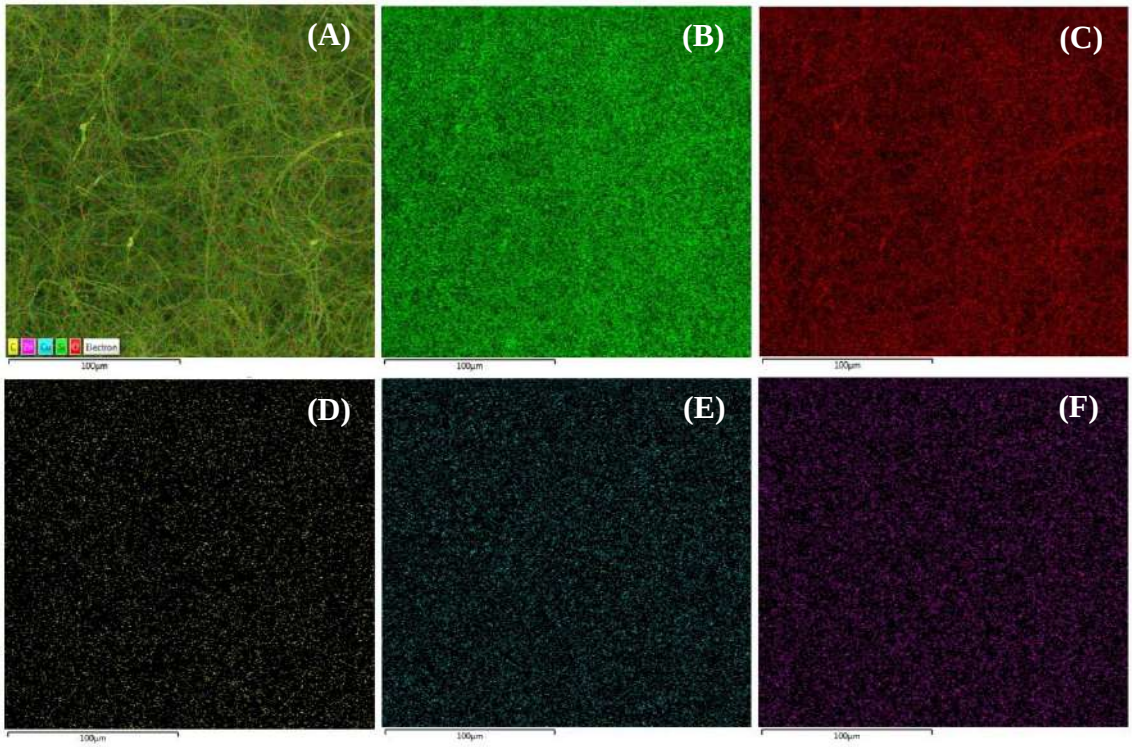

Figure 26 – EDX color mapping for 80Si10Zn10Cu: (A) General, (B) Silicon, (C) Oxygen, (D) Carbon, (E) Copper, (F) Zinc

5.5 Simulated body fluid test

In a first instance, four samples of each composition were prepared and immersed in SBF solution for 7 days. When it was attempted to remove the nanofiber samples from the containers, they could not be successfully collected. It was observed that the cylindrical samples fell apart before they could even be removed from the containers.

Figure 27 shows a sample of 80Si20Ca with 7 days of immersion prior to removal. At first glance, the samples appear to maintain their integrity (at the bottom of the container), however, when trying to remove them, they break easily.

Figure 27 – SBF test for 80Si20Ca after 7 days

Based on these complications, it was verified that the amount of SBF solution is correct for the sample volume. At the same time, immersions were performed again, but this time only for 1 day, with the objective of analyzing whether the residence time of the nanofibers in SBF could modify their stability to remove them from the container. After the experiment, the results were very similar. The samples did not fall apart as easily, but quickly enough to make it impossible to continue with the test.

Testing continued with a new preparation of the SBF solution, to corroborate that there were no problems related to this factor. Then, four samples of each composition were immersed for 1 day. After this period of time, an attempt was made to remove the samples from the containers, but first by pipetting out the SBF solution. Then, when the amount of SBF was considerably reduced, the samples were removed using tweezers again, but their poor integrity proved impossible to resolve.

A new test was performed, this time increasing the size of the samples (using a 7 mm puncher), using a larger diameter puncher to create larger cylinders, and correcting the amount of SBF needed for this case. The objective was to determine if perhaps the small size of the initial samples could be detrimental to performing such experiments successfully. After this modification, and again immersing four samples of each

composition in SBF for 1 day, it was confirmed that the samples broke down in the same way as in the previous cases.

In order to check the pH of the SBF solution for dissolution of the samples during their permanence into the solution, four samples of each composition were prepared and immersed for 7 days. Then, with a pH meter, the following values were taken as detailed in Table 8.

Table 8 – pH measurement after 1 day in SBF

Composition	**Sample number**			
	1	**2**	**3**	**4**
80Si20Ca	7.77	7.81	7.82	7.80
80Si18Ca2Zn	7.73	7.77	7.78	7.79
80Si18Ca2Cu	7.77	7.76	7.78	7.78
80Si16Ca2Zn2Cu	7.72	7.74	7.73	7.78
80Si15Ca5Zn	7.73	7.72	7.73	7.76
80Si15Ca5Cu	7.67	7.65	7.64	7.70
80Si10Ca5Zn5Cu	7.81	7.74	7.77	7.80
80Si10Zn10Cu	7.73	7.72	7.75	7.69

A slight increase in pH is observed compared to the SBF solution value (between 7.42-7.45). This could be related with a degradation of the bioactive glass in the solution, an exchange of ions could be occurring, but not further conclusions can be made. [15]

5.5.1 DMEM medium test

Considering the high concentration of ions present in the SBF solution that could affect the behavior of the nanofiber scaffolds after their immersion into the solution, the medium was changed to DMEM (Dulbecco's Modified Eagle Medium, Sigma-Aldrich, Germany), which is a widely used culture medium for cells and tissues in this type of applications. [29]

80Si20Ca samples were prepared with a 7 mm puncher and placed in a well-plate with a very low amount of DMEM medium, as can be seen in Figure 28 (A). The samples were then left for 1 day at 37°C and 100 rpm in an orbital shaker incubator. Also, same tests were performed for 80Si18Ca2Zn and 80Si18Ca2Cu.

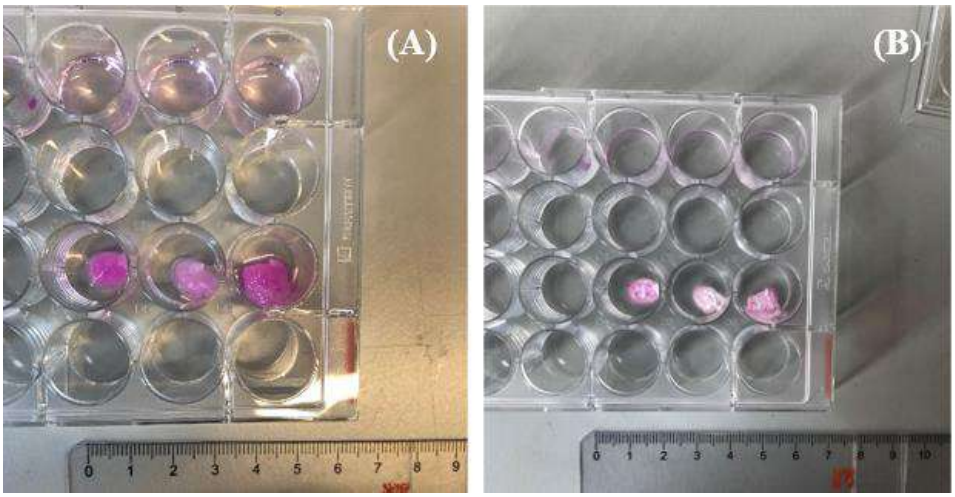

Figure 28 – 80Si20Ca samples in DMEM (A) Initial conditions (B) After 1 day

Figure 28 (B) shows the samples 24 hours later, where it can be seen that the samples adhered strongly to the well-plate and dried, making their extraction and subsequent characterization not possible. The same occurred with the other compositions tested.

5.6 Antibacterial test

The results of the antibacterial test can be seen in Figure 29 and Figure 30 for each type of bacteria. These studies are performed with two bacteria (*S. aureus* Gram-positive and *E. coli* Gram-negative) since these have differences in their cellular structure and therefore interact differently with antimicrobial agents. Consequently, it is important to test Zn- and Cu-doped scaffolds with both types of bacteria, which allows to better determine their overall efficacy as an antibacterial agent.

Eight measurements were made at 570 nm and the same amount at 600 nm for each of the compositions. Then, the Alamar Blue reductions were calculated according to Equation 1, and the averages and standard deviations were obtained. Finally, the results were normalized with respect to the control sample for each bacterium and then the graphs in Figure 29 and Figure 30 were plotted.

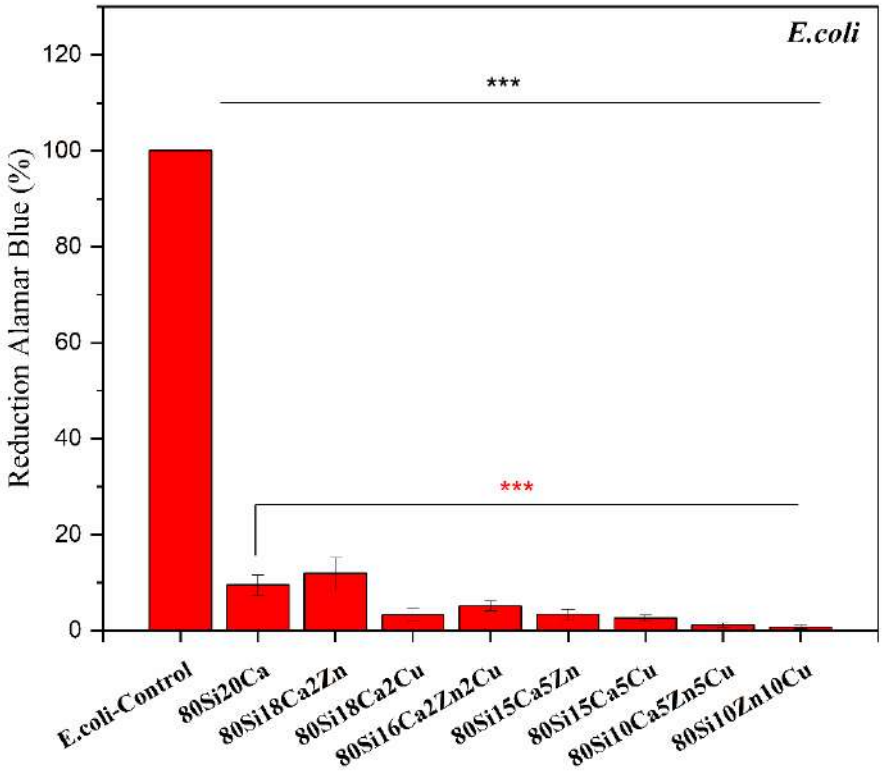

Figure 29 – Normalize Alamar Blue reduction for *E. coli*

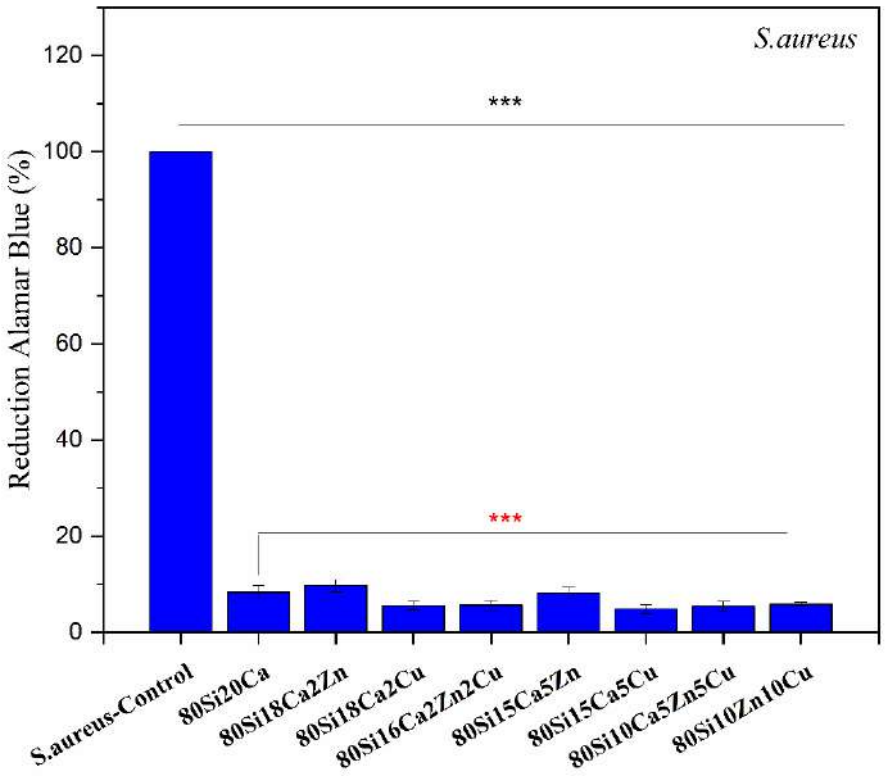

Figure 30 – Normalize Alamar Blue reduction for *S. aureus*

It was defined using "*" for each of the approved Bonferroni tests. In other words, each "*" represents a different significance level, within the three used (0.05, 0.01 and 0.001). As can be seen in Figure 29 and Figure 30, all compositions have “***”, then it could be verified that all the compositions satisfy the imposed condition. This indicates that the results obtained are not the product of chance, but are related to the variable studied, in this case the antibacterial properties of the scaffolds.

As for the results obtained, Figure 29 shows that the reductions of Alamar Blue are greater at lower ion concentrations, which means that as we increase the amount of Zn and Cu, the bacterial activity is reduced. This proves that Zn and Cu ions are good antibacterial agents, used for various biomedical applications. [30] [31] In addition, it can be said that there is a difference between BG 80Si20Ca scaffolds and compositions with Zn and Cu ions, especially for higher concentrations of these ions. No significant differences can be seen between compositions that include Zn versus compositions with Cu.

On the other hand, Figure 30 shows that for *S. aureus* bacteria, the antibacterial response is much more stable as we increase the amount of Zn and Cu ions. Again, better antibacterial results are observed for compositions including Zn and/or Cu, compared to 80Si20Ca.

Figure 31 compares bacterial growth using the solid agar plates for the 80Si20Ca and 80Si10Zn10Cu compositions. A greater presence of bacterial colonies can be clearly distinguished (due to the color change of the Alamar Blue) when there are no Zn or Cu ions in the sample, and a noticeable reduction when these ions are present. These results are consistent with the previous analysis.

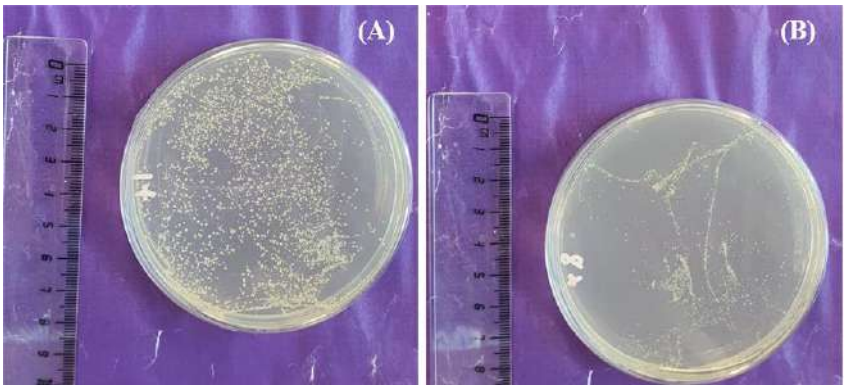

Figure 31 – Bacterial colonies for (A) 80Si20Ca and (B) 80Si10Zn10Cu

6. Conclusions

In view of the main objectives of this work, bioactive glass nanofiber scaffolds, doped with different amounts of zinc and copper ions, were successfully designed, prepared and electrospun, which allowed the definition of suitable fabrication parameters for this type of materials. These nanofiber scaffolds were obtained mostly in a 3D architecture, with their cotton-like appearance, as expected. The importance of certain parameters such as relative humidity or ambient temperature, concentrations of the components used and preparation times was noted. It could be inferred that these parameters are interrelated, so it is essential to work in the appropriate ranges of each of them in order to obtain the desired product.

Using SEM images, it was possible to study the morphology of the nanofibers, which were mostly defined as interconnected networks of homogeneous, bead-free fibers with a smooth surface. However, some beads could occasionally be identified in some of the samples, and also some fibers remained stuck together, even after the calcination heat treatment. These observed defects are related to the ES parameters, as well as to the solution preparation times, affecting solution viscosities. In addition, the average diameters were studied for each composition, where the decrease in size after HT, due to the removal of the polymer binding agent, was verified.

FTIR characterization allowed to corroborate the presence of the main functional groups for these bioactive glasses, as well as to confirm the removal of water, solvents, and the binder polymer PVB from the samples after HT. On the other hand, through EDX it was possible to confirm the presence of the expected chemical elements, as well as their mostly homogeneous spatial distribution from the study of the color maps. Also, with the EDX equipment software, it was verified that the composition originally designed for each sample remained stable at different spatial points.

The XRD tests did not show the typical amorphous glass halo of the Si-Ca system, as expected. Three hypotheses of possible contaminations were analyzed, concluding that probably the adhesive tape and sample holder could have interfered with the results. Despite this, the EDX and FTIR studies serve to confirm that the samples were not contaminated, so it was a problem in the preparation of the samples to be analyzed with the XRD equipment.

Bioactivity could not be evaluated, due to problems encountered during the experiments with SBF solution. Although several variables were tested, such as changes in the size of the samples, in the immersion times and in the medium used, it was not possible to remove any composition from its respective container, which made the subsequent planned characterization not possible.

Finally, the antibacterial properties were analyzed, with special attention to the presence of Zn and Cu ions, proving their good properties for this purpose. Reduced bacterial activities were recorded due to the presence of these ions, especially for *E. coli* bacteria, where the higher the concentration of these ions, the better the antibacterial properties were observed. Copper and zinc ions showed promising antibacterial results, which makes them interesting agents for biomedical applications, such as wound healing.

7. Future work

As future work, a series of activities can be proposed to optimize the results of this work, as well as other important complementary experiments for this type of bioactive glass materials. The most relevant points are detailed below.

- Repetition of XRD tests, trying a new sample preparation to place into the equipment, avoiding contamination from external agents.
- Focus on one selected composition at a time, in order to find the most optimal parameters and thus be able to study in depth the manufacturing variables and their influence on the quality of the final nanofibers.
- Repetition of SBF tests, working with larger sizes, in order to prevent samples from falling apart easily.
- Performance of cell proliferation and metabolic activity assays. [15]
- Incorporation of Ag ions to the study, considering the interest in these ions for their antibacterial properties. [31]
- Feasibility study for the realization of this type of nanofibers using 3D printers.

8. References

[1] Asadian, M., Chan, K. et al. (2019). Fabrication and Plasma Modification of Nanofibrous Tissue Engineering Scaffolds. Nanomaterials. DOI: 10.3390/nano10010119

[2] Chan, B., Leong, K. (2008). Scaffolding in tissue engineering: general approaches and tissue-specific considerations. European Spine. DOI: 10.1007/s00586-008-0745-3

[3] Venugopal, J., Low, S. et al. (2007). Interaction of Cells and Nanofiber Scaffolds in Tissue Engineering. Wiley Interscience. DOI: 10.1002/jbm.b.30841

[4] Negut, I., Dorcioman, G. et al. (2020). Scaffolds for Wound Healing Applications. Polymers Review. DOI: 10.3390/polym12092010

[5] Ratner, B., Hoffman, A. et al. (2004). Biomaterials Science: An Introduction to Materials in Medicine. 1. 1-20. ISBN: 008047036X, 9780080470368

[6] Ramakrishna, S., Fujihara, K. et al. (2006). Electrospun Nanofibers: Solving Global Issues. Journal Materials Today. 9. 40-50. DOI: 10.1016/S1369-7021(06)71389-X

[7] Memic, A., Abudula, T. et al. (2019). Latest Progress in Electrospun Nanofibers for Wound Healing Applications. American Chemical Society. DOI: 10.1021/acsabm.8b00637

[8] Rivero, G., Abraham, G. et al. (2021). Nanofibrous scaffolds for skin tissue engineering and wound healing applications. Tissue Engineering Using Ceramics and Polymers, Argentina. DOI: 10.1016/B978-0-12-820508-2.00020-9

[9] Pillay, V., Dott, C. et al. (2012). A Review of the Effect of Processing Variables on the Fabrication of Electrospun Nanofibers for Drug Delivery Applications. Journal of Nanomaterials. DOI: 10.1155/2013/789289

[10] Xue, J., Wu, T. et al. (2019). Electrospinning and Electrospun Nanofibers: Methods, Materials, and Applications. Chemical Reviews. DOI: 10.1021/acs.chemrev.8b00593

[11] Mit-uppatham, C., Nithitanakul, M. et al. (2004). Ultrafine Electrospun Polyamide-6 Fibers Effect of Solution Conditions on Morphology and Average Fiber Diameter. Macromolecular Chemistry and Physics. DOI: 10.1002/macp.200400225

[12] Liu, Y., Tian, Y. et al. (2014). CLSVOF method to study the formation process of taylor cone in crater-like electrospinning of nanofibers. Electrospun Polymer Nanomaterials: Preparation, Characterization, and Application. DOI: 10.1155/2014/635609

[13] Asmatulu, R. (2016). Highly Hydrophilic Electrospun Polyacrylonitrile/ Polyvinylpyrrolidone Nanofibers Incorporated with Gentamicin as Filter Medium for Dam Water and Wastewater Treatment. Journal of Membrane and Separation Technology. 5. 38-56. DOI: 10.6000/1929-6037.2016.05.02.1

[14] Baumgarten P.K. (1971). Electrostatic spinning of acrylic microfibers. Journal of Colloid and Interface Science, vol. 36, no. 1, pp. 71–79. DOI: 10.1016/0021-9797(71)90241-4

[15] Norris, E., Ramos-Rivera, C. et al. (2019). Electrospinning 3D bioactive glasses for wound healing. Biomedicals Materials, United Kingdom. DOI: 10.1088/1748-605X/ab591d

[16] Baino, F., Boccaccini, A. et al. (2015). Bioactive glasses: Special applications outside the skeletal system. Journal of Non-Crystalline Solids. DOI: 10.1016/j.jnoncrysol.2015.02.015

[17] Wang, D., Li, S. et al. (2014). Cotton-wool-like bioactive glasses for bone regeneration. Acta Biomaterialia, United Kingdom. DOI: 10.1016/j.actbio.2014.05.020

[18] Liverani, L., Reiter, T. et al. (2021). Copper-doped cotton-like malleable electrospun bioactive glass fibers for wound healing applications. Materials Letters. DOI: 10.1016/j.mlblux.2022.100133

[19] Ismail, A., van de Voort, F. et al. (1997). Fourier Transform Infrared Spectroscopy: Principles and Applications. Instrumental Methods in Food Analysis, Canada. Chapter 4, 93-95.

[20] Epp, J. (2016). X-ray diffraction (XRD) techniques for materials characterization. Materials Characterization Using Nondestructive Evaluation (NDE) Methods, Germany. Chapter 4, 81-124. DOI: 10.1016/B978-0-08-100040-3.00004-3

[21] Schindelin, J., Arganda-Carreras, I., Frise, E. et al. (2012) Fiji: an open-source platform for biological-image analysis. Nat Methods 9, 676–682. DOI: 10.1038/nmeth.2019

[22] Kokubo, T., Takadama, H. (2006). How useful is SBF in predicting in vivo bone bioactivity? Biomaterials, Japan. DOI: 10.1016/j.biomaterials.2006.01.017

[23] Haynes, W. (2013). Bonferroni Correction. Dubitzky, W., Wolkenhauer, O., Cho, KH., Yokota, H. Encyclopedia of Systems Biology. Springer, New York, NY. DOI: 10.1007/978-1-4419-9863-7_1213

[24] Gao, C., Gao, Q. et al. (2011). Preparation and In Vitro Bioactivity of Novel Mesoporous Borosilicate Bioactive Glass Nanofibers. Journal American Ceramic Society. DOI: 10.1111/j.1551-2916.2011.04434.x

[25] Xia, W., Zhang, D. et al. (2007). Fabrication and in vitro biomineralization of bioactive glass (BG) nanofibers. Journal of Nanotechnology, United Kingdom. DOI: 10.1088/0957-4484/18/13/135601

[26] Ju, Q., Zenji, T. et al. (2021). Silver-doped calcium silicate sol-gel glasses with a cotton-wool-like structure for wound healing. Materials and Science Engineering C. DOI: 10.1016/j.msec.2021.112561

[27] Akinci, Akin & Akbulut, Hatem & Yilmaz, Ferhat. (2007). The Effect of the Red Mud on Polymer Crystallization and the Interaction between the Polymer-Filler. Polymer-Plastics Technology and Engineering. 46. 31-36. DOI: 10.1080/03602550600916258

[28] JCPDS International Centre for Diffraction Data. (2019). PDF-4+ database. International Centre for Diffraction Data. Retrieved December 30, 2022, from https://www.icdd.com/

[29] Sigma-Aldrich. (2023). Dulbecco's Modified Eagle Medium (DMEM). Retrieved September 25, 2022, from https://www.sigmaaldrich.com

[30] Husheng, J., Wensheng, H. et al. (2005). The structures and antibacterial properties of nano-SiO2 supported silver/zinc–silver materials. Dental Materials. 24. 244-249. DOI: 10.1016/j.dental.2007.04.015

[31] Shimaburuko, M. (2020). Antibacterial Property and Biocompatibility of Silver, Copper, and Zinc in Titanium Dioxide Layers Incorporated by One-Step Micro-Arc Oxidation: A Review. Antibiotics Journal. DOI: 10.3390/antibiotics9100716

9. Acknowledgments

I would like to thank the Institute of Biomaterials at the Department of Materials Science and Engineering of the Friedrich-Alexander Universität (FAU) for allowing me to do my thesis, specially to Prof. Dr.-Ing. habil. Aldo Boccaccini, Dr. Liliana Liverani and Dr. Irem Ünalan for their constant support, help and dedication during my stay in Erlangen, Germany.

I would also like to thank the Universidad Nacional de Mar del Plata and specially Dr. Gustavo Abraham for his help, support and predisposition during the whole process.

To the I. DEAR program, and its coordinators Dr. Silvia Simison, Dr. Flavio Soldera, Dr. Andrea Camerucci, for their time and help during my experience.

Thank you to all the professors who were part of my time as a student, all of them were very important to me. Finally, to my family and friends, who made these years an enjoyable journey.

10. Appendix

10.1 Experimental conditions for the fabrication of BG nanofibers

10.1.1 80Si20Ca

80Si20Ca – 06/10/2021					
ES Parameters: 15 kV – 0.5 ml/h – 12 cm					
Start time (min)	**T_o (°C)**	**RH_o (%)**	**End time (min)**	**T_f (°C)**	**RH_f (%)**
17:55	22	36	18:15	21.6	37
18:18	21.9	37	18:38	21.5	36
18:41	21.5	36	19:01	21.3	37
80Si20Ca – 21/10/2021					
ES Parameters: 15 kV – 0.5 ml/h – 12 cm					
Start time (min)	**T_o (°C)**	**RH_o (%)**	**End time (min)**	**T_f (°C)**	**RH_f (%)**
10:40	23.2	32	11:00	23.5	31
11:02	23.5	32	11:22	23.8	32
11:24	23.8	32	11:34	23.8	32
80Si20Ca – 16/02/2022					
ES Parameters: 15 kV – 0.5 ml/h – 12 cm					
Start time (min)	**T_o (°C)**	**RH_o (%)**	**End time (min)**	**T_f (°C)**	**RH_f (%)**
10:11	23.9	27	10:31	23.9	27
10:33	23.8	27	10:53	23.9	28
10:55	23.9	28	11:15	23.9	28
11:17	23.7	28	11:37	23.8	28

10.1.2 80Si18Ca2Zn

80Si18Ca2Zn – 07/10/2021
ES Parameters: 15 kV – 0.5 ml/h – 12 cm

Start time (min)	T_o (°C)	RH_o (%)	End time (min)	T_f (°C)	RH_f (%)
16:05	22.6	32	16:25	22.6	33
16:28	22.6	33	16:48	22.6	33
16:50	22.6	33	17:10	22.4	34
17:12	22.4	34	17:32	22.4	34
17:34	22.4	34	17:54	22.4	34
80Si18Ca2Zn – 20/10/2021					
ES Parameters: 15 kV – 0.5 ml/h – 12 cm					
Start time (min)	**T_o (°C)**	**RH_o (%)**	**End time (min)**	**T_f (°C)**	**RH_f (%)**
11:38	23.5	37	11:58	23.8	37
12:00	24	37	12:20	24	37
12:22	24	37	12:42	24.2	37
12:44	24.2	37	13:07	24.2	36
80Si18Ca2Zn – 29/10/2021					
ES Parameters: 15 kV – 0.5 ml/h – 12 cm					
Start time (min)	**T_o (°C)**	**RH_o (%)**	**End time (min)**	**T_f (°C)**	**RH_f (%)**
10:51	23.9	30	11:11	24.2	30
11:13	24.2	30	11:33	24.2	30
11:35	24.2	30	11:55	24.2	30
11:57	24.4	30	12:17	24.4	30
12:19	24.4	30	12:39	24.4	30
12:41	24.4	30	13:01	24.4	30

10.1.3 80Si18Ca2Cu

80Si18Ca2Cu – 11/11/2021					
ES Parameters: 15 kV – 0.5 ml/h – 12 cm					
Start time (min)	**T_o (°C)**	**RH_o (%)**	**End time (min)**	**T_f (°C)**	**RH_f (%)**
11:10	23.7	27	11:30	23.9	27

11:32	23.9	27	11:52	23.9	27
11:54	24.2	27	12:14	24.2	27
12:16	24.2	27	12:36	24.2	27
12:38	24.2	27	12:58	24.2	27
13:00	24.4	27	13:20	24.4	27
13:21	24.4	27	13:41	24.4	27
80Si18Ca2Cu – 17/11/2021					
ES Parameters: 15 kV – 0.5 ml/h – 12 cm					
Start time (min)	**T_o (°C)**	**RH_o (%)**	**End time (min)**	**T_f (°C)**	**RH_f (%)**
13:45	24.2	29	14:05	24.4	28
14:07	24.4	28	14:27	24.4	28
14:29	24.4	28	14:49	24.4	28
14:51	24.4	28	15:11	24.4	28

10.1.4 80Si16Ca2Zn2Cu

80Si16Ca2Zn2Cu – 25/11/2021					
ES Parameters: 15 kV – 0.5 ml/h – 12 cm					
Start time (min)	**T_o (°C)**	**RH_o (%)**	**End time (min)**	**T_f (°C)**	**RH_f (%)**
12:26	23.4	27	12:46	23.7	26
12:48	23.7	27	13:08	23.9	26
13:10	23.9	26	13:30	23.9	26
13:31	23.9	26	13:51	24.2	26
80Si16Ca2Zn2Cu – 18/02/2022					
ES Parameters: 15 kV – 0.5 ml/h – 12 cm					
Start time (min)	**T_o (°C)**	**RH_o (%)**	**End time (min)**	**T_f (°C)**	**RH_f (%)**
9:58	23.9	29	10:18	24.2	28
10:20	24.2	28	10:40	24.4	28
10:41	24.4	28	11:01	24.4	28
11:03	24.4	28	11:23	24.6	28

11:24	24.6	28	11:44	24.6	28
11:45	24.4	29	12:05	24.4	29

10.1.5 80Si15Ca5Zn

80Si15Ca5Zn – 01/12/2021					
ES Parameters: 15 kV – 0.5 ml/h – 12 cm					
Start time (min)	**T_o (°C)**	**RH_o (%)**	**End time (min)**	**T_f (°C)**	**RH_f (%)**
12:37	23.5	28	12:57	23.7	28
12:59	23.7	29	13:19	23.7	29
13:21	23.7	29	13:41	23.7	29
13:43	23.7	29	14:03	23.8	29
80Si15Ca5Zn – 19/01/2022					
ES Parameters: 15 kV – 0.5 ml/h – 12 cm					
Start time (min)	**T_o (°C)**	**RH_o (%)**	**End time (min)**	**T_f (°C)**	**RH_f (%)**
11:00	23.5	26	11:20	23.7	26
11:22	23.5	26	11:42	23.7	26
11:43	23.7	26	12:04	23.7	26
12:05	23.7	26	12:25	23.7	26
12:27	23.7	26	12:47	23.7	26
12:49	23.7	26	13:09	23.7	26
13:10	23.7	26	13:30	23.9	26

10.1.6 80Si15Ca5Cu

80Si15Ca5Cu – 02/12/2021					
ES Parameters: 15 kV – 0.5 ml/h – 12 cm					
Start time (min)	**T_o (°C)**	**RH_o (%)**	**End time (min)**	**T_f (°C)**	**RH_f (%)**
11:45	23.5	28	12:05	23.9	28
12:07	23.9	28	12:27	24.2	28
12:28	23.9	28	12:48	23.9	28

12:50	24.2	28	13:10	24.2	27
80Si15Ca5Cu – 26/01/2022					
ES Parameters: 15 kV – 0.5 ml/h – 12 cm					
Start time (min)	**T_o (°C)**	**RH_o (%)**	**End time (min)**	**T_f (°C)**	**RH_f (%)**
14:15	24.2	26	14:35	24.2	26
14:37	24.2	26	14:57	24.2	26
14:59	24.2	26	15:19	24.2	26
15:21	24.2	26	15:47	24.2	26
15:50	24.2	26	16:13	24.2	26

10.1.7 80Si10Ca5Zn5Cu

80Si10Ca5Zn5Cu – 26/11/2021					
ES Parameters: 15 kV – 0.5 ml/h – 12 cm					
Start time (min)	**T_o (°C)**	**RH_o (%)**	**End time (min)**	**T_f (°C)**	**RH_f (%)**
12:19	23.7	27	12:39	23.7	27
12:40	23.7	27	13:00	23.9	27
13:02	23.9	27	13:22	23.9	27
13:24	23.9	27	13:44	23.9	26
80Si10Ca5Zn5Cu – 23/02/2022					
ES Parameters: 15 kV – 0.5 ml/h – 12 cm					
Start time (min)	**T_o (°C)**	**RH_o (%)**	**End time (min)**	**T_f (°C)**	**RH_f (%)**
10:13	23.9	28	10:33	23.9	28
10:34	23.9	28	10:54	24.4	28
10:56	24.4	28	11:14	24.4	27
11:17	24.4	27	11:37	24.4	27
11:39	24.4	27	11:59	24.6	27
12:00	24.6	27	12:35	24.6	27

10.1.8 80Si10Zn10Cu

80Si10Zn10Cu – 20/01/2022					
ES Parameters: 15 kV – 0.5 ml/h – 12 cm					
Start time (min)	**T_o (°C)**	**RH_o (%)**	**End time (min)**	**T_f (°C)**	**RH_f (%)**
10:59	23.7	27	11:18	23.7	27
11:20	23.7	27	11:40	23.7	27
11:41	23.7	27	12:01	23.7	27
12:03	23.7	27	12:23	23.9	27
12:25	23.9	27	12:45	23.9	26
80Si10Zn10Cu – 24/02/2022					
ES Parameters: 15 kV – 0.5 ml/h – 12 cm					
Start time (min)	**T_o (°C)**	**RH_o (%)**	**End time (min)**	**T_f (°C)**	**RH_f (%)**
10:15	23.5	29	10:35	23.5	29
10:37	23.5	29	10:57	23.5	28
10:59	23.5	28	11:21	23.6	28